Response to Referee #3

We thank the referee for their review and their thoughtful comments. Point-to-point responses can be found below, and the relevant changes have been made to the manuscript.

General comments:

Comment #1(a)

The introduction could be considerably reduced without harming its quality: the general introduction in wind energy (up until line approx. line 27) can be omitted, the discussion on induction control could be reduced to simply mentioning that dynamic control is much more promising than static (with some key references, i.e. Annoni et al, Campagnolo et al, Munters & Meyers, Frederik et al.)

Response
We will streamline the introduction review.

Comment #1(b)
The literature review at the beginning of Section 2.2 can be shortened

Response
We will shorten the literature review for brevity.

Comment #1(c)
Section 2.4 basically discusses a straightforward time lag based on Taylor's hypothesis. This could be significantly shortened.

Response
We will remove this section and state the time lag based on Taylor's hypothesis in a brief fashion.

Comment #1(d)
Section 2.5 takes up quite a lot of space with again a detailed review, but very little is said related to the current manuscript, other than 'the update frequency is selected according to the dynamics of the problem studied'. Further, 'Comments on the update frequency are made in Section 5.' (l. 270), hinting on a study where the sensitivity to this frequency is analyzed, where is this exactly? Or do the authors refer to the part where a dynamic approach is compared to a lookup table (i.e. Section 5.1)? In the latter case, please rephrase (l. 270) more exactly.

Response
We will streamline and re-phrase the discussion in Section 2.5 and on Line 270 to improve clarity.

Comment #2(a)

It would be illustrative if the authors could provide a schematic which shows inputs, outputs, and operations of the algorithm. This could be similar to figure 1 which shows α and γ as inputs to the state estimation, however their role is not discussed in section 2.2.

Response
We will include a schematic to describe the state estimation methodology and clarify the role of α and γ.

Comment #2(b)
Further, the statement 'The EnKF is computationally superior ... but this may lead to spurious correlations in the state representation' is somewhat confusing. Does this affect the results in the current paper?

Response
We will remove the statement which does not directly relate to the results of the current paper.

Comment #2(c)
The EnKF is particularly well-suited for discretized PDE problems. Why? add a suitable reference perhaps

Response
We will remove this statement which is not critical to the current paper.

Comment #2(d)
The outcome of the EnKF is a vector with k w and σ for all turbines except the last one, for which this is not relevant (l 191 p 7). However, in your equations, this last turbine is included in the state estimation, e.g. see Equation (7). Is this correct?

Response
Thank you for noting this notation error. The referee is correct that the furthest downwind turbine does not need to be included in the state estimation, and in fact, its parameters are irrelevant for the wake model. We will adjust the state estimation equations accordingly.

Comment #2(e)
Equation (18): should all π's be replace with $\hat{}\pi$ here? If not, how is π defined?

Response
Thank you for noting this typographical error in Equation (18). The π's should have been ψ's and we have fixed the error.

Comment #3(a)
The authors use an actuator disk model. Some more details would be welcome. Is it a rotating or non-rotating model (I assume the latter). The ADM is accurate in the far wake, yet at a turbine spacing of 4D it is doubtful whether far wake conditions are met. Somme comments on

this would be welcome. How does the ADM deal with the dependency of thrust forces and power extraction on yaw angle? Is this a standard cos 2 (γ) and cos 3 (γ) respectively? How does this influence conclusions based on the sensitivity of the control framework on P p in section 5.3?
G

Response

The actuator disk model used in the large eddy simulations presented in this study does not include rotation, it is a standard actuator disk model. We will include more details on the ADM in the manuscript and the description is also stated here. The referee is correct to note that the ADM has some discrepancy with the rotating ALM in the near-wake region.

To be clear, the relative turbine spacing in the conventionally neutral ABL simulations is between 4-5D in the mean hub-height wind direction since the spacing is 4D in the x-direction and the turbines are aligned at 18 degrees to the x-axis.

The wind speed profile at the wind turbine hub height approximately 4D downwind of the leading turbine, incident on the second turbine, is shown in Figure 1. The wake profile exhibits a Gaussian shape, rather than a top-hat shape, suggesting that with the turbulence intensity and length scales present in the conventionally neutral ABL LES, 4-5D spacing is sufficient to establish far wake behavior with the actuator disk model used in this study. This is consistent with the expected location of far-wake behavior onset (experimentally found in yawed rotating turbines to be approximately x/D=3 [1]).

The goal of the current study is to test the efficacy of the closed-loop control algorithm, and therefore, the focus was not to precisely match the wakes observed in full-scale wind farms through LES; future work should also incorporate more advanced wind turbine models.

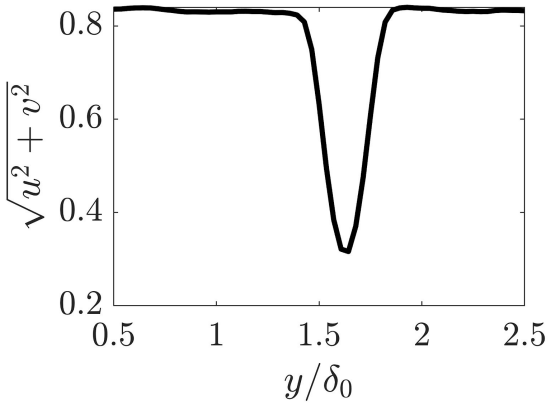

Figure 1: Time averaged wind speed profile at x/δ_0=3.5 at the wind turbine hub height. The flow at this x-location is incident on the second wind turbine in the array. The wind speed exhibits a Gaussian profile, suggesting the onset of far-wake behavior [see e.g. 1].

Within the actuator disk model formulation, the dot product is taken between the incident wind velocity vector and the wind turbine rotor normal vector to calculate the perpendicular velocity vector. The thrust force normal to the rotor area is computed using the perpendicular velocity, the axial induction factor (a=0.25), and the coefficient of thrust ($C_T = 0.75$ in the

current study). The forces are then projected into the computational domain coordinate system. In this fashion, the dependence of the thrust force (with thrust being defined as parallel to the mean velocity at hub height) on the yaw misalignment angle is $cos^2(\gamma)$ given uniform inflow conditions. Importantly, with non-uniform flow conditions, the thrust is not guaranteed to follow $cos^2(\gamma)$. The ADM power production is defined as $P = u_p \cdot F_T$ where u_p is the velocity perpendicular to the rotor area and F_T is the thrust force. This results in a power production dependency on the yaw misalignment angle of $cos^3(\gamma)$, again, for uniform inflow conditions only. For heterogeneous flow conditions, the scaling for thrust and power as a function of yaw misalignment is approximately $cos^2(\gamma)$ and $cos^3(\gamma)$, respectively, although it may deviate from these approximate scaling expectations. We will include further comments on the ADM in the revised manuscript.

The particular "ground-truth" value of P_p, as discussed in Section 5.3, is wind turbine model specific. The current LES experiments detail the sensitivity of the wind farm power production, and therefore the efficacy of wake steering, to the estimate of P_p for a ground-truth $P_p = 3$, but the sensitivities noted in the current study are not expected to depend on the particular ground-truth value for P_p. For example, the current experiments show that an estimate of $P_p = 2$ when the ground-truth value is 3 leads to power production loss compared to standard operation. For a different wind turbine model with a ground-truth of $P_p = 2$, we would then expect an estimate of $P_p = 1.5$ may lead to undesirable results, for example, while $P_p = 2$ would be an excellent estimate. The results of the current study are not absolute, in the sense that $P_p = 4$ is always a good choice, but relative, in the sense that a conservative estimate for P_p is wise given the P_p parameter uncertainty which is present in wake steering applications. We have refined the discussion in Section 5.3 to clarify this point.

Comment #3(b)
p.12, l 323 – 325: '... without the influence of variable turbine operation, the flow is identical to machine precision between yaw aligned and yaw misaligned cases'. I would suggest rephrasing this. I understand the authors want to convey that both cases are started from identical initial conditions, and any differences can hence be attributed to differences in farm controls. However, stating that these simulations are 'identical to machine precision' is somewhat deceptive in the simulation of a chaotic dynamical system. In such systems, differences (even at machine precision levels e.g. by adapting compiler optimization levels), will grow exponentially in time, resulting in a completely different turbulent flow realization. I'm not saying this is the case in the current simulations, but a better phrasing would simply be to remove the 'to machine precision' part.

Response
Thank you for this comment. The referee is correct that differences in turbulent systems grow exponentially in time and even modifications in the compiler optimization could cause these differences which grow to O(1) errors. We have carefully ensured that these floating-point differences are eliminated by fixing the initialization (to machine precision), compiler optimization, and processor topology in the present study to allow for quantitatively rigorous

comparisons between the various control simulations. We have added a footnote to clarify the points the referee has raised.
We can further demonstrate the point the referee has raised here. We perform a numerical experiment with three simulations. In the conventionally neutral LES flow, we fix all parameters and initializations to machine precision and the control architecture is fixed between the three cases. In two cases (#1 and #2), the processor topology is fixed while in the third case (#3), the compiler optimization changes the processor topology. The power production for Cases #2 and #3 normalized by the power from Case #1 are shown below in Figure 2. Cases #1 and #2 remain in quantitative agreement to machine precision while Cases #1 and #3 diverge. The deviation between Cases #1 and #3 are a consequence of round-off differences that occur due to global reduction (sum) operations with modified processor topology.
All comparison cases in this paper were performed with the comparison methodology enforced in Cases #1 and #2.

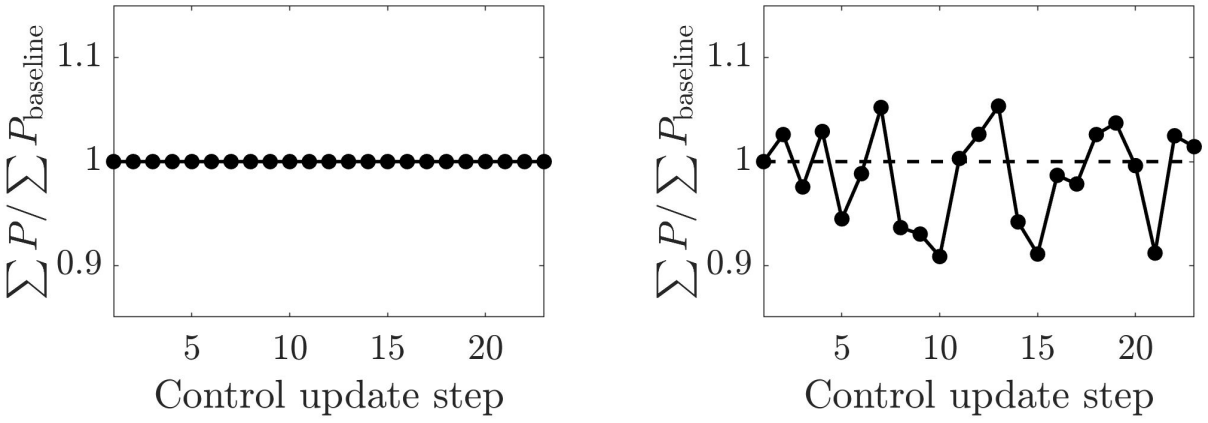

Figure 2: Processor topology experiment. In the left plot, the wind turbine array power production (Case #2) is normalized by a separate LES case (Case #1) with fixed control architecture and initialization as well as a fixed processor topology. In the right plot, the power (Case #3) is normalized by a separate LES case with fixed control architecture and initialization but a modified processor topology (Case #1). The normalized power from Case #3 oscillates around 1 as a function of time.

Comment #4(a)
The relatively low grid resolution, combined with the uniform inflow creates a possibly problematic setup where the wake behind the first turbine is artificially stabilized, resulting in very low baseline power in row 2, and hence huge gains to be obtained from any type of control. A remark could be added to the text on this. This is somewhat mentioned in l. 361, but it would be good to mention that this case is highly dependent on things like grid resolution, SGS model, and hence physical results should be interpreted with care.

Response

Thank you for this comment. The referee is correct that LES of uniform inflow impinging on wind turbine models at typical LES resolutions leads to an artificial stabilization as mentioned in the discussion in Section 4 (Line 361). This challenge of turbulent transition in wind turbine model wakes for uniform inflow and the influence of the SGS model was discussed in detail in Howland *et al JRSE* (2016) [2]. As a result of this comment, and those of the other referees, we have moved the uniform inflow test case section to the Appendix to reduce confusion between this unphysical algorithmic test case and the physical conventionally neutral LES results.

Comment #4(b)
Figure 3 and Figure 4: x-axis is labeled time step. Is this simulation time step of control update step? I'm suspecting the latter, but it would be better to be explicit, similar to how axes are labeled in later figures.

Response
Thank you for noting this typographical error. The x-axes for Figures 3 and 4 should state 'Control update step,' and we have updated the manuscript accordingly.

Comment #4(c)
p. 14, l. 369: The authors indicate their fear of an overparametrized model which is overfitting by spurious anti-correlation of k w and σ 0 . Would it make sense / be possible to directly try and obtain these parameters from a time-averaged LES flow field and hence quantify the 'correct' parameter values?

Response
Thank you for this suggestion. This is an interesting idea and it is possible to quantify an empirical best-fit for the wake spreading rate kw in the LES setting. In fact, this has been the previous wake modeling approach to the wind farm controls problem (see e.g. Niayifar & Porte-Agel (2015) [3] and the FLORIS model). However, this methodology is impractical in a field setting for continuous parameter estimation where nacelle-mounted LiDARs are not often available and *a priori* parameterized values for physical constants can lead to inaccurate power predictions (see comparison with empirical Gaussian wake model in Figure 21). The purpose of the present study is to establish a framework which relies only on readily available SCADA data for model parameter estimation, and therefore we have not focused on flow-field empirical parameter fitting in this study. Future work should investigate the efficacy of physics-based constraints during optimization of the wake model parameters, but this is out of the scope of the current study.

Comment #4(d)
Concluding, the overall added value of this section is quite limited in my opinion. The main contribution would be to have a very basic test case, showing that the EnKF and yaw angles are relatively stable for steady flow conditions. Therefore, I believe it would be better if the section is introduced and discussed with this aim.

Response

As discussed in the response to **Comment #4(a),** we have moved this section to the Appendix to focus on the physical results in the conventionally neutral ABL setting.

Comment #5(a)
Table 1 is introduced early on. However, by itself, the table is insufficiently explained to completely understand which case is which. An example is the NA case, which is not clearly defined in the text until Appendix C. Also, the naming and order in which these cases are presented in the table could be greatly improved. For example, Section 5.1 discusses NL and ND2, whereas ND1 is only introduced in Section 5.2. The naming also gets very confusing later on, e.g. the case with P p = 2 is called ND4 and P p = 4 is called ND5. This results in the reader constantly having to go back to Table 1 to recall which case is which. More logical naming would prevent this, e.g. replace ND4 by NDP2, ND5 by NDP4.

Response
We will describe the cases and Table 1 in more detail and earlier in the manuscript to improve clarity and we have re-named the cases according to the referee's suggestions. Note that we have also switched the names of Case ND1 and ND2 in the revision as per the referee's suggestion.

Comment #5(b)
The final column in Table 1 is used to determine statistical significance of improvements over the basecase. It would be more illustrative to plot this in a barplot including errorbars, because seeing whether these values overlap for different cases from numerical data is not trivial.

Response
Thank you for this suggestion, we have incorporated a barplot (Figure 5) with corresponding errorbars to clarify these data and their statistical significance.

Comment #5(c)
Section 5.1: How is the lookup table in the NL case generated? Is this simply by running 1 control window, and then keeping the yaw angles constant? How robust is this? I.e. how would these steady yaw angles differ if they were generated based upon a state estimation from a different time window / turbulent flow realization? This would have an impact on statistical significance of the results.

Response
As discussed on Line 416 of the manuscript, the lookup table approach is approximated by:
"The lookup table control is approximated by fixing the yaw misalignment angles as a function of time after the initial optimal angles are computed during the first yaw controller update"

Generating the yaw angles in a different time window would lead to small changes in the yaw misalignment values computed by the model-based optimizer as the referee has mentioned. This point was investigated by the authors extensively before submission of the manuscript, although it was not shown for brevity in the already lengthy manuscript. We will articulate the results here and add a brief discussion in the revised manuscript.

While generating yaw misalignment angles in a different time window/turbulent flow realization with slightly different mean wind direction, wind speed, turbulence intensity, etc leads to slightly different values of yaw misalignment, the conclusions of the study are not affected since the changes to the wind farm power production are not statistically significant. This experiment was investigated for Case ND1 and Case ND1R, the robustness version of Case ND1 which is algorithmically identical but initialized at a later LES temporal instance.

The yaw misalignment values implemented in the first control update step of Case ND1 are (from first to last turbine in degrees):
[16.8163, 17.0334, 16.8953, 14.7568, 2.8090, 0.0000]
The increase in power production over baseline control (Case NA) is for Case ND1: 4.59% +/- 2.34%
The yaw misalignment values for Case NL are identical to the first step of Case ND1 by definition.

In a robustness test case, the conventionally neutral ABL LES is run for several more physical hours before the yaw misalignment strategy is switched on the and resulting yaw misalignment values are computed in the separate turbulent time window realization (from first to last turbine in degrees):
[15.5785, 15.8899, 14.4753, 12.1178 , 3.7497, 0.0000]
Case ND1 was repeated, starting from the later time, and the increase in power production over baseline control (Case NAR, which was also re-run for the later time window) is for Case ND1R: 5.7% +/- 2.03%
The yaw misalignment values for Case NLR are identical to the first step of Case ND1R by definition. Therefore, changing the time window for the lookup table approximation did not significantly change the yaw misalignment values, as the referee has suggested.

The differences in power production for these two cases are not statistically significant as characterized by a one-sided two-sample Kolmogorov-Smirnov test at a 5% significance level. Further, the yaw misalignment values are qualitatively and quantitatively similar. Therefore, while the specific time wind in which the lookup table (or dynamic yaw) control is implemented has some influence on the quantitative results, we have demonstrated that it does not influence the statistical significance of the results. We have added a discussion in the manuscript to clarify this point.

Comment #5(d)
Section 5.1: p. 18, l. 438. a lot of explanation is given for a non-significant performance difference. Does this make sense?

Response
We will modify the discussion to highlight that the result is not statistically significant.

Comment #5(e)

For figures like 8,9,10,11, it would improve direct interpretability of the figures if the case name was included directly on the plot instead of only in the caption. There is ample whitespace left to do this everywhere.

Response
We will add the case numbering to the plots.

Comment #5(f)
Section 5.2: p. 22, l. 492 the authors claim 'The most successful dynamic control framework ... is the static state estimation methodology'. Please add the casename here explicitly (ND3 I presume). Based on what metric is ND3 more successful than ND2? Power extraction differences were mentioned not to be significant.

Response
As with **Comment #5(d)**, we will limit the differentiation of cases which are not statistically significant differences.

Comment #5(g)
Section 5.2: p. 23, l.496: 'This potential dependence of k w and σ 0 on yaw misalignment was not incorporated explicitly ...' Is this dependence not implicitly accounted for through the EnKF?

Response
This is an excellent observation by the referee. The goal of the data-driven EnKF methodology is that the dependence is implicitly accounted for. The authors were suggesting that future work could also incorporate this dependence explicitly in a physics-based modeling strategy. We will clarify this in the manuscript.

Comment #5(h)
Section 5.2 last paragraph: This comparison to NL lookup table seems a bit out of place. Could this be moved to Section 5.1? I understand there are chronological dependencies in how you want to write down observations, but the current narrative is somewhat confusing.

Response
Thank you for this suggestion, we have reformulated the narrative to improve clarity.

Comment #5(i)
Section 5.3 p.25, l.532: 'Interestingly, ND5 outperforms ND2, but not significantly' This statement is confusing, if its insignificant, then the outperformance is not to be distinguished from statistical noise, so calling that interesting seems contradictory. Please remove or rephrase

Response
As with **Comment #5(d),** we will remove discussion of statistically insignificant results.

Comment #5(j)

Section 5.4: the part on FLORIS can probably be omitted. Further, this section basically also quantifies a dependence on P p , which was already the subject of Section 5.3. Consider renaming sections to avoid overlap in their definition.

Response
The authors believe that a comparison with an empirical physics-based model without state estimation is warranted to show the benefit of the EnKF on power production predictions. The lifting line model has not received an empirical calibration treatment as the Gaussian wake model has [see ref. 2], and therefore FLORIS was selected as a comparison. It is important to note that this comparison is predominantly a commentary on the success of the EnKF for improving wake model state estimation, rather than a comparison between the lifting line and Gaussian wake models.

Minor/technical comments:

Comment #1
The title of the paper could be improved such that the goal of the research is reflected therein, namely quantifying the sensitivity to design choices in the control framework. Currently, the title 'Optimal closed-loop wake steering' is rather generic, and mentioning that it is 'part 1' of a two-parts paper in my opinion degrades the idea that the current work is self-contained.

Response
Thank you for this comment. This article was titled 'Part 1' since there will be a follow-up 'Part 2' which will focus on wake steering in diurnal cycle simulations. Each article will be self-contained, as the present article is.

Comment #2
p.3, l.79: mentioning that accurately predicting greedy base-line power production is the main challenge in wake steering control, is somewhat exaggerated in my opinion.

Response
We will modify the language in the manuscript to highlight that dynamic wake steering does indeed carry other technical challenges aside from the mentioned baseline power production prediction.

Comment #3
The output of your controller is a time-series of yaw angles γ(t), do the ADM in the LES directly impose these yaw angles, or is there a limitation on the yaw rates? Figure 3 seems to indicate a very large jump in yaw angle within a single timestep. Is this technically feasible?

Response
Yaw control rates are typically ~0.5°/s. The largest jump in yaw misalignment in the present study is from greedy control to wake steering control in 'Control update step 1' of the simulations. This jump has a maximum of 30°, which would take approximately 60 seconds to implement. This time is significantly less than the Taylor's hypothesis time lag (Section 2.4) and therefore this yaw rate will not influence the results. For a dynamic wake steering controller with a more rapid yaw update frequency, this effect should be considered.
This was discussed in the original manuscript on Line 480 but we have moved the discussion to the LES formulation Section 3 to improve clarity.

Comment #4
p.7, l. 184: number of turbines N T , l. 192: number of turbines N t (either use N T or N t)

Response
We will fix the typographical error.

Comment #5
p.9, l.234: I believe the algorithm should be denoted as Adam, not ADAM

Response
We will fix the typographical error.

Comment #6
p.10,l.280: add the continuity equation to the momentum equation

Response
We will add the continuity equation for completeness.

Comment #7
p.10,l.264: psuedo vs. pseudo?

Response
Pseudo, we will fix the typographical error.

Comment #8
Figure 2 and Figure 6 could be improved by adding a snapshot of a velocity field in addition to the purely schematic domain presentation.

Response
We will add a velocity field snapshot.

Comment #9
p.13,l.345: in incorporated vs is incorporated

Response
We will fix the typographical error.

Comment #10
p.20,l.471: proportionality constant σ 0

Response
Thank you, we will adjust the manuscript accordingly.

Comment #11
p.21,l.472: Gaussian wake does NOT have a clear trend

Response
We will fix the typographical error.

References

[1] Bastankhah, M., and F. Porté-Agel. "Wind tunnel study of the wind turbine interaction with a boundary-layer flow: Upwind region, turbine performance, and wake region." *Physics of Fluids* 29.6 (2017): 065105.

[2] Howland, Michael F., et al. "Wake structure in actuator disk models of wind turbines in yaw under uniform inflow conditions." *Journal of Renewable and Sustainable Energy* 8.4 (2016): 043301.

[3] Niayifar, Amin, and Fernando Porté-Agel. "A new analytical model for wind farm power prediction." *Journal of physics: conference series*. Vol. 625. No. 1. IOP Publishing, 2015.

Optimal closed-loop wake steering, Part 1: Conventionally neutral atmospheric boundary layer conditions

Michael F. Howland[1], Aditya S. Ghate[2], Sanjiva K. Lele[1,2], and John O. Dabiri[3,4]

[1]Department of Mechanical Engineering, Stanford University, Stanford, CA 94305
[2]Department of Astronautics and Aeronautics, Stanford University, Stanford, CA 94305
[3]Graduate Aerospace Laboratories of the California Institute of Technology (GALCIT), California Institute of Technology, Pasadena, CA 91125
[4]Department of Mechanical and Civil Engineering, California Institute of Technology, Pasadena, CA 91125

Correspondence: John O. Dabiri (jodabiri@caltech.edu)

Abstract. Strategies for wake loss mitigation through the use of dynamic closed-loop wake steering are investigated using large eddy simulations of conventionally neutral atmospheric boundary layer conditions, where the neutral boundary layer is capped by an inversion and a stable free atmosphere. The closed-loop controller synthesized in this study consists of a physics-based lifting line wake model combined with a data-driven Ensemble Kalman filter (EnKF) state estimation technique to calibrate the wake model as a function of time in a generalized transient atmospheric flow environment. Computationally efficient gradient ascent yaw misalignment selection along with efficient state estimation enables the dynamic yaw calculation for real-time wind farm control. The wake steering controller is tested in a six turbine array embedded in a statistically quasi-stationary conventionally neutral flow with geostrophic forcing and Coriolis effects included. The controller statistically significantly increases power production compared to baseline, greedy, yaw-aligned control ~~although the magnitude of success of the controller depends on the state estimation architecture and the wind farm layout~~provided that the EnKF estimation is constrained and informed with a physics-based prior belief of the wake model parameters. The influence of the model for the coefficient of power C_p as a function of the yaw misalignment is characterized. Errors in estimation of the power reduction as a function of yaw misalignment are shown to result in yaw steering configurations that under-perform the baseline yaw aligned configuration. Overestimating the power reduction due to yaw misalignment leads to increased power over greedy operation while underestimating the power reduction leads to decreased power, and therefore, in an application where the influence of yaw misalignment on C_p is unknown, a conservative estimate should be taken. ~~Sensitivity analyses on the controller architecture, coefficient of power model, wind farm layout, and atmospheric boundary layer state are performed to assess benefits and trade-offs in the design of a wake steering controller for utility-scale application. The physics-based wake model with data assimilation~~ The EnKF-augmented wake model predicts the power production in yaw misalignment with a mean absolute error over the turbines in the farm of $0.02P_1$, with P_1 as the power of the leading turbine at the farm~~, whereas a physics-based~~. A standard wake model with wake spreading based on an empirical turbulence intensity relationship leads to a mean absolute error of $0.11P_1$, demonstrating that state estimation improves the predictive capabilities of simplified wake models.

1 Introduction

~~Wind and solar energy are likely the only low-carbon energy technologies which are being implemented rapidly enough to mitigate the effects of global warming (IEA, 2017). Since wind energy has a low marginal cost (Bitar et al., 2012), increases in wind farm power production approximately manifest as a reduction in the levelized cost of electricity (LCOE) (Joskow, 2011). While the LCOE of wind energy is already often below those of traditional combined-cycle natural gas and coal (Bilgili et al., 2015; EIA, 20~~
~~, continued reductions in wind energy LCOE will likely increase the adoption of this technology (Borenstein, 2012; Ouyang and Lin, 2014) due to improved economics in sub-optimal wind resource areas (Wiser et al., 2015).~~ Modern horizontal axis wind turbines achieve performance approaching the Betz limit (Wiser et al., 2015). However, collections of wind turbines arranged in wind farms suffer from aerodynamic interactions which reduce wind farm power production between 10 and 20% (Barthelmie et al., 2009) due to greedy control schemes which only consider the power maximization of individual wind turbines at the farm. Recent work has focused on the operation of wind turbines in a collective fashion in order to increase the power production of the wind farm through the mitigation of wake interactions (see review by Boersma et al., 2017).

Wind farm power optimization through wake interaction mitigation methods have generally relied on axial induction and yaw misalignment control since these two methodologies do not require significant hardware modifications on traditional horizontal axis wind turbines (Burton et al., 2011). ~~Annoni et al. (2016) utilized a steady-state model to inform the optimal axial induction factors for each wind turbine in an LES of a model wind farm but did not find significant power production improvements over baseline greedy operation. Campagnolo et al. (2016a) found similar results in a wind tunnel experiment of three wind turbines. The full large eddy simulation (LES) adjoint equations were used to optimize the power production by Goit and Meyers (2015). Munters and Meyers (2017) and Munters and Meyers (2018) extended the work of Goit and Meyers (2015) and used dynamic axial induction and yaw misalignment to increase wind farm power production using the full-state adjoint. While these studies achieved successful dynamic power production increases over baseline operation, the computational expense of adjoint LES is similar to standard LES and is currently a challenge to use in real-time wind farm control. Bauweraerts and Meyers (2019) showed that coarse LES can potentially be used for real-time prediction and control but this requires future investigation and is not the focus of the present study. Ciri et al. (2017) used a model-free formulation and dynamic control to increase the power production of a model wind farm and found that downstream wind turbines may also need to change their operational strategy to increase farm performance. Gebraad et al. (2013) also used a model-free gradient-based optimizer to increase the power production of a wind farm by approximately 1%. Park and Law (2016) used data-driven Bayesian ascent to efficiently maximize the power production of a model wind farm using axial induction . As a general conclusion of the present literature, simulations and field experiments of stationary axial induction based on static-wake models (models which represent the time averaged behavior of a stationary or quasi-stationary flow) have shown this methodology is unlikely to increase~~ Readers are directed to Knudsen et al. (2015) and Kheirabadi and Nagamune (2019) for recent reviews of wind farm power ~~production in utility-scale wind farms but may improve wind turbine fatigue loading provided that the objective function is carefully proposed~~

and the fatigue is accurately modeled (see extensive review by Knudsen et al., 2015). Meanwhile, maximization methodologies. Previous simulation studies have shown that wake steering may have more potential than static axial induction control for wind farm power maximization (Annoni et al., 2016; Gebraad et al., 2016a; Campagnolo et al., 2016a), although dynamic axial induction (Park and Law, 2016; Munters and Meyers, 2018; Frederik et al., 2020) or more sophisticated dynamic blade pitch strategies (Frederik et al., 2019) may significantly increase power production (Munters and Meyers, 2018; Frederik et al., 2019, 2020) and require future field experimentation.

Greedy wind turbine operation minimizes the yaw misalignment between the nacelle position and the incoming wind direction. Contemporary wind turbines often operate in small yaw misalignment due to sensor noise and uncertainty (Fleming et al., 2014) leading to sub-optimal power production for the misaligned turbine. However, recent attention has focused on wake steering, the intentional misalignment of certain turbines within a wind farm in order to deflect wakes laterally away from downwind generators (Grant et al., 1997; Jiménez et al., 2010). While the yaw misaligned wind turbine's power production is decreased (Burton et al., 2011; Medici, 2005)(Medici, 2005; Burton et al., 2011), wake steering has been shown to increase the power production of downwind generators in simulations (Fleming et al., 2016; Gebraad et al., 2017; Fleming et al., 2018; Archer and Vasel-Be-Hagh, 2019) and wind tunnel experiments (Adaramola and Krogstad, 2011; Mühle et al., 2018; Bastankhah and Porté-Agel, 2019). Further, the potential for wake steering to increase wind farm power production in wind conditions with wake losses has been observed in full-scale field campaigns with two (Fleming et al., 2017, 2019) and six wind turbines (Howland et al., 2019).

While wake steering has been shown to be a beneficial global wind farm control strategy compared to greedy operation, the selection of the optimal yaw misalignment strategy for each wind turbine at a farm is challenging. The optimal yaw misalignment angles depend on the wake interactions between wind turbines (Gebraad et al., 2017). These wake interactions are dependent on wind speed, wind direction, atmospheric stability, turbulence intensity, local terrain, and other flow features (see e.g. Hansen et al., 2012). Most wake steering control strategies have relied on static engineering wake models such as the FLORIS model (Gebraad et al., 2016a, b; Fleming et al., 2016) or a lifting line model (Shapiro et al., 2018; Howland et al., 2019) to select the optimal yaw misalignment strategy based on a steady, time-averaged assumption of the wind farm flow. Extremum seeking wake steering control has also been tested by Campagnolo et al. (2016b) using a gradient-based controller. However, these static model approaches may have challenges in establishing the optimal yaw misalignment strategy as a function of time in a transient flow environment such as the stable atmospheric boundary layer (ABL) or the full diurnal cycle (see e.g. Wyngaard, 2010).

Recent work has focused on the selection of the optimal yaw misalignment angles as a function of time for transient flow applications. The main challenge in this flow environment Ciri et al. (2017) used a model-free formulation and dynamic control to increase the power production of a model wind farm in simulations. While model-free optimization is the subject of promising on-going work, this methodology generally experiences slower rates of convergence and may be less suited to transient flow applications where wind conditions shift rapidly, although future work should compare model-based and model-free formulations in transient flow applications. A significant challenge in transient flow environments is in accurately predicting the power production given greedy baseline control, considering ABL and controller state uncertainty in a utility-scale wind

farm. The ~~combined two-dimensional computational fluid dynamics and adjoint-based optimization model WFSim has been utilized (see e.g. Boersma et al., 2016, 2018; Vali et al., 2019) for control applications. Subsequent studies have used the~~ Ensemble Kalman filter (EnKF) has been leveraged to perform model state estimation as a function of time (Doekemeijer et al., 2017) ~~. The EnKF filter has been successfully used~~ and for low-order model state estimation for the purpose of receding horizon frequency regulation control (Shapiro et al., 2017) and reference power signal tracking applications (Shapiro et al., 2019). Doekemeijer et al. (2018) found that the EnKF has comparable state estimation performance given either nacelle-mounted LiDAR data or Supervisory Control and Data Acquisition (SCADA) power production data alone. Since very few utility-scale wind turbines have nacelle-mounted LiDAR systems, the successful performance of the EnKF based on SCADA data alone highlights the potential for online model calibration without additional hardware installation. ~~The present computational complexity of the EnKF-WFSim system may limit the applicability to real-time control systems, although recent efforts have focused on the reduction of the simulation time of this method. As such, real-time closed-loop wind farm controllers with online state estimation require reliable analytic wake models such as the FLORIS or lifting line model.~~

Static wake model based dynamic control studies have utilized a quasi-static wake steering approach wherein the optimal yaw misalignment angles are computed and stored as a function of wind speed and direction based on static wake models with pre-defined model parameters (Fleming et al., 2019). However, the pre-defined model parameters were calibrated for the ~~FLORIS wake model~~ Gaussian wake model (Bastankhah and Porté-Agel, 2014) based on idealized ~~LES~~ large eddy simulations (LES) and their applicability to a new utility-scale field implementation are unknown *a priori*. Further, there is additional uncertainty associated with the freestream velocity and turbulence intensity measurements in a wind farm environment where the typical sensors are limited to nacelle-mounted anemometers placed directly behind the rotating rotor. The dynamic influence of yaw misalignment on these sensors is unknown (Howland et al., 2019). Recently, Raach et al. (2019) used the FLORIS wake model to design a closed-loop wake steering controller which relies on a downwind facing nacelle-mounted LiDAR system which was able to increase power production in an example nine wind turbine LES case. In order to focus on a low-order methodology which does not require additional hardware installations, we develop closed-loop wake model based wake steering control for the application of data-driven wind farm power maximization based on SCADA power production data. The algorithm was designed for real-time control of utility-scale wind turbines without the requirement of additional hardware or sensor measurement systems and utilizes the gradient-based optimal yaw algorithm developed by Howland et al. (2019). The dynamic wake steering controller implemented in this study does not require historical data to be sorted into pre-selected wind speed and direction bins in order to make optimal yaw misalignment decisions. This is beneficial since the sorting of SCADA data represents a major uncertainty associated with wake steering control (Fleming et al., 2019; Howland et al., 2019).

Analytic wake models require a number of simplifications of the flow physics and wind turbine operation in order to predict wind farm power production in a computationally efficient fashion (see e.g. review by Stevens and Meneveau, 2017). However, compared to model-free control, the wake model encodes a prior belief of the physics of wind farm flows and establishes a base performance given the initial model parameters preceding the perturbations applied by the EnKF (also see discussion by Schreiber et al., 20 . The selected model-based optimal yaw misalignment angles will depend on the wake deflection model form and parameters, and the model for power production degradation as a function of the yaw misalignment angle. Further, in a low-order, model-

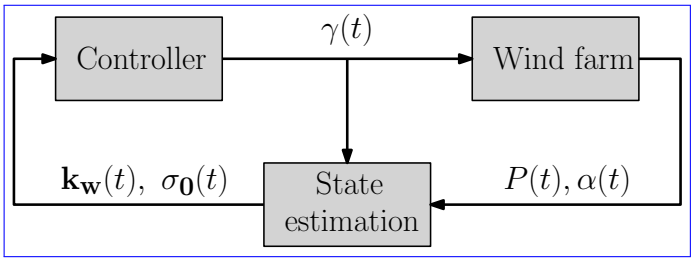

Figure 1. Diagram of the dynamic wake steering control system. The wake model parameters as a function of time are $k_w(t)$ and $\sigma_0(t)$ and the yaw misalignment angles are given by $\gamma(t)$. The power production and wind direction are given by $P(t)$ and $\alpha(t)$, respectively. In open-loop control, the model parameters k_w and σ_0 are fixed as a function of time.

driven power optimization application, the selected yaw misalignment angles will depend on the wind farm layout, wind direction and speed, and stability state of the ABL. The goal of the present study is to analyze the sensitivity of wind farm power production ~~increases through wake steering as a function of~~ to the design of the control system, model for power loss as a function of yaw misalignment, and wind farm layout ~~.~~ when leveraging wake steering control.

This work represents Part 1 of the results and targets a canonical planetary boundary layer with conventionally neutral stratification. Part 2 will focus on a sensitivity analysis of wake steering control ~~as a function of the~~ with temporally varying stratification and surface heat flux. Section 2 will introduce the dynamic wake steering methodology and EnKF state estimation technique. The LES methodology is introduced in Section 3. The dynamic wake steering ~~will be~~ is validated in a two-turbine uniform inflow LES case in ~~Section~~ Appendix F. In Section 4, the sensitivity to model architecture and parameters ~~as well as wind farm layout~~ is tested in LES of the conventionally neutral ABL with realistic Coriolis forcing. Finally, conclusions are given in Section 5.

2 Dynamic wake steering methodology

The present methodology is focused on optimal closed-loop wake steering control as a function of time for transient flow applications. The dynamic wake steering controller is illustrated in Figure 1. The controller entails a forward-pass wake model described in Section 2.1 and a backward pass to compute analytic gradients for gradient-ascent power maximization (Section 2.3). State estimation uses the ensemble Kalman filter described in Section 2.2. The wind farm is simulated using LES (Section 3). The closed-loop control algorithm and implementation is validated in Appendix F for LES of uniform inflow.

2.1 Lifting line wake model

Following the observation of counter-rotating vortex pairs shed by wind turbines operating in yaw misalignment in experiments and LES ~~(Howland et al., 2016)~~(Mikkelsen et al., 2003; Howland et al., 2016; Bastankhah and Porté-Agel, 2016), Shapiro et al. (2018) developed a wake model for wind turbines in yaw based on Prandtl's lifting line theory. The wake model derived by Shapiro et al. (2018) was reformulated by Howland et al. (2019) to improve computational efficiency and to extract analytic

gradients for the purpose of gradient-based optimization. Readers are directed to Shapiro et al. (2018) for the derivation of the initial wake model and to Howland et al. (2019) for the analytic formulation which eliminates the need for domain discretization. In the two dimensional static wake model, the rotor averaged effective velocity at a downwind wind turbine j is given as

$$u_{e,j}(x) = u_\infty - \sum_i^{N_f} \frac{\sqrt{2\pi}\delta u_i(x) d_{w,i}(x) D}{16\sigma_{0,i}} \left[\text{erf}\left(\frac{y_T + D/2 - y_{c,i}(x)}{\sqrt{2}\sigma_{0,i} d_{w,i}(x)} \right) - \text{erf}\left(\frac{y_T - D/2 - y_{c,i}(x)}{\sqrt{2}\sigma_{0,i} d_{w,i}(x)} \right) \right], \tag{1}$$

where u_∞ is the incoming freestream velocity and δu_i and $d_{w,i}$ are the velocity deficit and the wake diameter as functions of x associated with the upwind turbine i, respectively. The wind turbine rotor diameter is given by D. The downwind turbine lateral centroid is y_T and the lateral wake centroid is $y_{c,i}$. The wake model parameters are k_w, the wake spreading coefficient and σ_0, the proportionality constant for the presumed Gaussian wake. The velocity deficit trailing a single wind turbine is

$$\delta u_i(x) = \frac{\delta u_{0,i}}{d_{w,i}^2(x)} \frac{1}{2} \left[1 + \text{erf}\left(\frac{x}{\sqrt{2} D/2} \right) \right], \tag{2}$$

with $\delta u_{0,i} = 2 a_i u_\infty$ and axial induction factor $a_i = 1/2 \left(1 - \sqrt{1 - C_{T,i} \cos^2(\gamma_i)} \right)$. The thrust coefficient is given by C_T and the yaw misalignment angle is given by γ. The wake model assumes the thrust force in the streamwise direction $T \sim \cos^2(\gamma)$ which may not be valid for all wind turbine models (see e.g. Bastankhah and Porté-Agel, 2016). In the present LES cases, the wind turbine model enforces this thrust scaling (see §3) and therefore sensitivity analyses on this assumption are left for future work. Positive and negative yaw misalignment are defined as counter-clockwise and clockwise rotations, respectively, when viewed from above. ~~The inflow wind angle is given by α, where 0° is north and proceeds clockwise to 360° at north again. The thrust force in the streamwise direction is assumed to follow actuator disk theory as $\cos^2(\gamma)$. The~~ The wake diameter as a function of the streamwise location x is $d_{w,i}(x) = 1 + k_{w,i} \log\left(1 + \exp[2(x/D - 1)]\right)$. Linear superposition of the individual wakes is assumed in Eq. 1 (Lissaman, 1979).

The wake centerline $y_{c,i}$ is given by

$$y_{c,i} = \int_{x_{0,i}}^{x} \frac{-\delta v_i(x')}{u_\infty} dx', \tag{3}$$

where the spanwise velocity δv is given similar to Eq. 2 with the initial disturbance given analytically as (Shapiro et al., 2018)

$$\delta v_{0,i} = \frac{1}{4} C_{T,i} u_\infty \cos^2(\gamma_i) \sin(\gamma_i). \tag{4}$$

The wind turbine model power is computed as

$$\hat{P}_i = \frac{1}{2} \rho A_i C_p u_{e,i}^3, \tag{5}$$

where A is the wind turbine rotor area and ρ is the density of the surrounding air. The model for the coefficient of power C_p as a function of the yaw misalignment remains an open question. Often, the power loss as a function of the yaw misalignment is assumed to follow $P_{\text{yaw}} \sim P \cos^{P_p}(\gamma)$, where P_p is a known parameter. Following actuator disk theory (Burton et al., 2011),

$P_p = 3$. However, simulations have shown for the NREL 5 MW turbine that $P_p = 1.88$ (Gebraad et al., 2016a). Recent work has shown that P_p differs for freestream and waked turbines ~~(?)~~(Liew et al., 2020). The value of P_p that results in a satisfactory agreement with experimental data depends on the wind turbine model, ABL shear and veer, and atmospheric stability. In the present study, we will consider P_p an uncertain parameter and perform sensitivity analysis on it. The uncertainties of the wake model parameters k_w and σ_0 are considered by the state estimation in Section 2.2. The coefficient of power is modeled as

$$C_{P,i} = 4\eta a_{p,i}(1 - a_{p,i})^2 \cos^{P_p}(\gamma_i), \tag{6}$$

with $a_{p,i} = \frac{1}{2}\left(1 - \sqrt{1 - C_{T,i}}\right)$ The parameter η is tuned to match the manufacturer provided yaw-aligned C_P look-up table (Gebraad et al., 2016a). The applicability of this model is limited to Region II of the wind turbine power curve which is typically between 4 and 15 m/s.

2.2 Ensemble Kalman filter state estimation

Engineering wake models rely on parameters which represent physical phenomena, such as the wake spreading rate k_w. ~~Niayifar and Porté-Agel (2016) proposed the dependence of k_w on the turbulence intensity which may be measured at a wind farm by nacelle anemometers, and this model has been used in subsequent FLORIS applications (see e.g. Fleming et al., 2018) . Shapiro et al. (2019) proposed the use of canonical turbulent wake mixing and a prescribed mixing length model to estimate k_w. Schreiber et al. (2019) utilized a data-driven approach where error terms are added to the engineering model and SCADA is used for data assimilation to correct the wake model inaccuracies.~~ Gradient optimization-based SCADA data assimilation was used by Howland et al. (2019) to select the model parameters which minimize the model error in producing the site-specific wind farm greedy baseline power production. Howland and Dabiri (2019) subsequently used gradient descent coupled with a genetic algorithm for data assimilation.

Here, we will employ the EnKF (Evensen, 2003) state estimate technique along with the wake model described in Section 2.1. The EnKF filter was found to be computationally less expensive than the gradient-based data assimilation used by Howland et al. (2019). ~~The EnKF filter is computationally superior to other Kalman filter methods (extended, unscented, etc.) since there are typically fewer ensemble states than dimensions but this may lead to spurious correlations in the state representation (see e.g. discussion by Doekemeijer et al., 2018; Mandel, 2009). The states~~ The states and dimensions here represent the wake model instantiations and parameters, respectively. In our state estimation case, the dimension space scales linearly with the number of turbines ~~N_T~~ N_t, rather than with the ~~N_T^2 or N_T^3~~ N_t^2 or N_t^3 in a model with a domain discretization (see discussion by Howland et al., 2019). ~~Therefore the number of ensembles, which is a hyperparameter selected by the EnKF user, and dimensions will be of the same order of magnitude.~~ The SCADA power production of each wind turbine is a function of time, denoted P_k, where k is the time step index. The goal is to estimate the wake model parameters given SCADA power production data measurements, $P_k \in \mathbb{R}^{N_t}$, using the ensemble Kalman filter as a rapid gradient-free optimizer (Cleary et al., 2020). This approach follows previous uses of the EnKF for wake model state estimation (Shapiro et al., 2017; Doekemeijer et al., 2017) but the algorithm is reviewed here. The ~~EnKF is particularly well-suited for discretized partial differential equation systems, often in geophysical applications, and is computationally efficient for the present application as well~~ nonlinear wake model,

denoted by h, also receives the wind speed and direction from the leading turbine, as well as the yaw misalignment of each turbine in the farm. There are two wake model parameters for each upwind turbine and no parameters for the last turbine downwind. The model parameters with N_t wind turbines at the k^{th} time step are given by

$$\psi_k = [k_{w,1}, ..., k_{w,N_t} \; w,N_t-1, \sigma_{0,1}, ..., \sigma_{0,N_t} \; 0,N_t-1]. \tag{7}$$

The modeling and measurement errors are represented by ~~$\chi = [\chi_{k_w}^T, \chi_{\sigma_0}^T]^T \in \mathbb{R}^{2N_t}$~~ $\chi = [\chi_{k_w}^T, \chi_{\sigma_0}^T]^T \in \mathbb{R}^{2(N_t-1)}$ and $\varepsilon \in \mathbb{R}^{N_t}$, respectively. The modeling errors χ_{k_w} and χ_{σ_0} are zero mean and have prescribed variances of $\sigma_{kw}^2 = 0.0009$ and $\sigma_{\sigma_0}^2 = 0.0009$. The Gaussian random measurement noise ε has zero mean and a prescribed standard deviation of $\sigma_\varepsilon = 0.03 \cdot P_1$. The hyperparameter variances were selected based on tuning experiments (see Appendix A). In order to estimate the state model parameters, the EnKF ~~filter~~ uses an ensemble of wake model evaluations. The ensemble is given by

$$\Psi = [\psi^{(1)}, ..., \psi^{(N_e)}] \in \mathbb{R}^{2N_t \times N_e} \; 2(N_t-1)\times N_e. \tag{8}$$

The power predictions are given by the matrix

$$\hat{\Pi} = [\hat{\pi}^{(1)}, ..., \hat{\pi}^{(N_e)}] \in \mathbb{R}^{N_t \times N_e}, \tag{9}$$

where N_e is the number of ensembles.

The statistical noise of the power production measurements is given by ε. The Gaussian random noise is added to the SCADA measurements for each ensemble

$$\xi^{(i)} = P_{\text{data}} + \varepsilon^{(i)}. \tag{10}$$

The perturbed power production ensemble matrix is

$$\Xi = [\xi^{(1)}, ..., \xi^{(N_e)}] \tag{11}$$

with the perturbation matrix prescribed by

$$\Sigma = [\varepsilon^{(1)}, ..., \varepsilon^{(N_e)}] \tag{12}$$

The mean of the ensemble states and modeled power production is given by

$$\overline{\Psi} = \Psi \mathbf{1}_{N_e} \tag{13}$$

$$\overline{\hat{\Pi}} = \hat{\Pi} \mathbf{1}_{N_e} \tag{14}$$

where $\mathbf{1}_{N_e} \in \mathbb{R}^{N_e \times N_e}$ is a full matrix where all entries are $1/N_e$. The perturbation matrices are

$$\Psi' = \Psi - \overline{\Psi} \tag{15}$$

$$\hat{\Pi}' = \hat{\Pi} - \overline{\hat{\Pi}}. \tag{16}$$

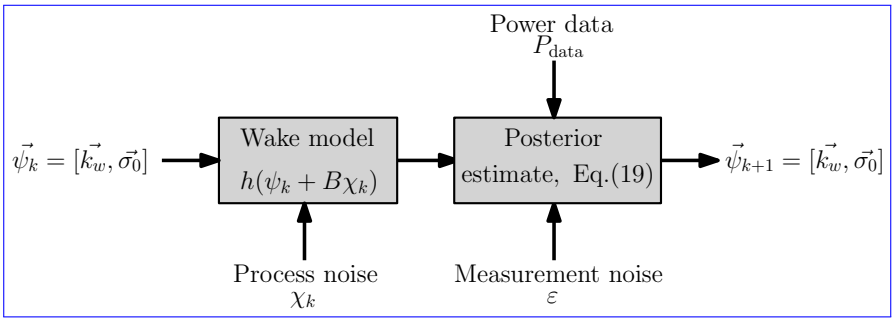

Figure 2. Schematic of the ensemble Kalman filter parameter estimation methodology. The wake model predicts the power production given wake model parameters ψ_k from time step k and the modeled process noise χ. The power data from the LES are augmented with modeled measurement noise ε. The wake model predictions, $h(\psi_k + B\chi_k)$, process and measurement noise, and power data are leveraged to compute the parameters in the $k+1$ time step ψ_{k+1} using the measurement analysis step (Eq. 19).

The first step in the EnKF process is an intermediate forecast step

$$\Psi_{k+} = [\psi_k^{(1)} + B\chi_k^{(1)}, ..., \psi_k^{(N_e)} + B\chi_k^{(N_e)}] \tag{17}$$

$$\hat{\Pi}_{k+} = [h(\pi\psi_k^{(1)} + B\chi_k^{(1)}), ..., h(\pi\psi_k^{(N_e)} + B\chi_k^{(N_e)})]. \tag{18}$$

where matrix ~~$B \in \mathbb{R}^{2N_t \times 2N_t}$~~ $B \in \mathbb{R}^{2(N_t-1)\times 2(N_t-1)}$ is the identity matrix and h represents the nonlinear wake model described in Section 2.1.

The measurement analysis step is given by

$$\Psi_{k+1} = \Psi_{k+} + \Psi'_{k+}\hat{\Pi}'^T_{k+}(\hat{\Pi}'_{k+}\hat{\Pi}'^T_{k+} + \Sigma_{k+1}\Sigma^T_{k+1})^{-1} \cdot (\Xi_{k+1} - \hat{\Pi}_{k+}). \tag{19}$$

The final values of k_w and σ_0 for the $k+1$ time step are given as the columns of $\overline{\Psi}_{k+1}$. The EnKF is repeated for a predefined number of iterations for improved estimation (see Appendix A). The EnKF state estimation then assumes that the parameters $k_{w,k+1}$ and $\sigma_{0,k+1}$ will be valid over the succeeding finite time from step $k+1$ until step $k+2$. A schematic of the EnKF methodology is shown in Figure 2.

The EnKF is a Kalman filter method which uses the Monte-Carlo sampling of model parameters according to a prescribed Gaussian function to represent the covariance matrix of the probability density function (PDF) of the state vector Ψ. The likelihood of the data is represented using observations Ξ and prescribed perturbations Σ. Using the prior PDF of the state (k) and data likelihood, the posterior state ($k+1$) is estimated using Bayes's rule (Eq. 19).

2.3 Optimal yaw misalignment optimization

The optimal yaw misalignment angles depend on the wind speed, direction, turbulence intensity, and other key ABL conditions. Within a given condition bin, the number of potential yaw misalignment angle combinations grows exponentially with the number of wind turbines. As such, brute force optimization methods are not sufficient for the selection of the optimal yaw

misalignment strategy. Previous studies have considered genetic algorithms (Gebraad et al., 2016a), discrete gradient-based optimization (Gebraad et al., 2017), and analytic gradient-based optimization (Howland et al., 2019). Using gradient-based ~~ADAM~~ Adam optimization (Kingma and Ba, 2014), the gradient update is given by

$$\gamma^{t+1} = \gamma^t - \alpha \frac{m_t}{\sqrt{v_t}}, \tag{20}$$

where $m^t = \beta_1 m^{t-1} + (1-\beta_1)\frac{\partial \sum \hat{P}}{\partial \gamma}$ and $v^t = \beta_2 v^{t-1} + (1-\beta_2)(\frac{\partial \sum \hat{P}}{\partial \gamma})^2$. The hyperparameters are set to the commonly used values of $\beta_1 = 0.9$ and $\beta_2 = 0.999$, respectively (Kingma and Ba, 2014). The analytic gradients computed by Howland et al. (2019) are used for the gradient-based wind farm power optimization.

2.4 ~~Approximate advection timescale~~

~~Upon the yaw misalignment of an upwind turbine, there is a time lag associated with the advection time scale of the flow for the control decision to influence a downwind turbine. While the advection time depends on the length scale of the turbulent eddy (Del Álamo and Jiménez, 2009; Yang and Howland, 2018; Howland and Yang, 2018), the mean flow advection approximately follows the mean wind speed in wind farms (Taylor, 1938; Lukassen et al., 2018). The number of simulation time steps associated with the approximate advection time between the first and last turbines is computed as~~

~~$$T_{\mathrm{a}} = \frac{\Delta s_x}{\overline{u}_{\mathrm{hub}} \Delta t},$$~~

~~where Δs_x is the distance between the first and last turbine in the streamwise direction and $\overline{u}_{\mathrm{hub}}$ is the mean streamwise velocity at the wind turbine model hub height at the leading turbine in the farm. The simulation time step is fixed and is Δt, which corresponds to a CFL of less than 1 persistently during runtime. In the computation of wind farm statistics for the utilization of static wake models, the advection time scale is accounted for by initializing the time averaging two advection time scales $2T_a$ after the yaw misalignments for the wind turbine array have been updated. To account for errors associated with the simple advection model, the time lag is taken as double the advection time scale, $2T_a$. The sensitivity of the wind farm power production and model-predicted optimal yaw misalignment angles as a result of the advection time lag are considered in Section 4.~~

2.4 ~~Yaw misalignment temporal update frequency~~

~~While static wake models are able to capture time averaged wind farm dynamics in stationary flows (see e.g. Stevens and Meneveau, 2017) , instantaneous wind speed and direction are constantly changing and challenging to predict. As the stability of the atmosphere transitions during the diurnal cycle, the mean wind conditions as well as turbulence intensity will change with a significant impact on the wake loss magnitude (Hansen et al., 2012). The wake steering strategy must be dynamic to adapt to the instantaneous wind conditions but also requires some time lag according to the advection time scale of the wind farm. The selection of the optimal yaw misalignment angle update frequency will impact the power production of the wind farm. Kanev (2020) found that when utilizing a dynamic wake steering controller in transient flow environments the energy production may decrease as~~

~~a result of wind direction fluctuations as a function of time. The energy loss was due to the dynamic wake steering controller attempting to follow the wind direction constantly as a function of time, leading to increased yaw duty, and a final yaw update time of 2 minutes was selected.~~

~~In a full-scale wake steering field experiment, Fleming et al. (2019) found that wind direction and speed data low pass filtering resulted in an unintended time lag between the observed conditions and the associated optimal yaw misalignment angles. Finally, Raach et al. (2019) utilized a feedforward-feedback framework to adjust the open-loop predicted optimal yaw misalignment angles continuously based on LiDAR measurements of the wake centroid location, instead of SCADA power measurements, with an update time scale on the order of seconds. In the present study, the yaw misalignment update frequency is selected according to the dynamics of the problem studied. Comments on the update frequency for the conventionally neutral ABL LES cases are made in Section 4.~~

3 Large eddy simulation setup

Large eddy simulations are performed using the open-source ~~psuedo-spectral~~ pseudo-spectral code *PadéOps*[1]. The solver uses 6^{th} order compact finite differencing in the vertical direction (Nagarajan et al., 2003) and Fourier collocation in the horizontal directions. Temporal integration uses a fourth order strong stability preserving Runge-Kutta variant (Gottlieb et al., 2011). The LES code has previously been utilized for high Reynolds number ABL flows (Howland et al., 2020a; Ghaisas et al., 2020) and is described in detail by Ghate and Lele (2017). The ABL is modeled as an incompressible, high Reynolds number limit ($Re \to \infty$) flow with the filtered, nondimensional momentum equations given by

$$\frac{\partial u_i}{\partial t} + u_j \frac{\partial u_i}{\partial x_j} = -\frac{\partial p}{\partial x_i} - \frac{\partial \tau_{ij}}{\partial x_j} + f_i + \frac{\delta_{i3}}{Fr^2}(\theta - \theta_0) - \frac{2}{Ro}\varepsilon_{ijk}\Omega_j u_k - \frac{\partial P^G}{\partial x_i},$$

$$\frac{\partial u_i}{\partial t} + u_j \frac{\partial u_i}{\partial x_j} = -\frac{\partial p}{\partial x_i} - \frac{\partial \tau_{ij}}{\partial x_j} + f_i + \frac{\delta_{i3}}{Fr^2}(\theta - \theta_0) - \frac{2}{Ro}\varepsilon_{ijk}\Omega_j u_k - \frac{\partial P^G}{\partial x_i},$$

(21)

$$\frac{\partial u_i}{\partial x_i} = 0$$

(22)

where u_i is the velocity in the x_i direction, p is the nondimensional pressure, and P^G is the nondimensional geostrophic pressure. The subfilter scale stress tensor is given by τ_{ij} and the sigma model is employed (Nicoud et al., 2011). The turbulent Prandtl number used in the subfilter scale model is $Pr = 0.4$ (Ghate and Lele, 2017). Surface stress and heat flux is computed using a local wall model based on Monin-Obukhov similarity theory with appropriate treatment based on the state of stratification (Basu et al., 2008). The wind turbine forcing is represented by f_i and ~~an~~ a non-rotating actuator disk model is used (Calaf et al., 2010). The actuator disk thrust force acts parallel to the rotor normal vector. The incident velocity is projected into the rotor disk plane and therefore the dependence of thrust on the yaw misalignment γ in uniform inflow

[1] https://github.com/FPAL-Stanford-University/PadeOps

conditions would be $\cos^2(\gamma)$, although it may deviate from this in sheared and veered inflow conditions. While the actuator disk model is lower fidelity than the actuator line methods, it captures the far wake (far wake is approximately $x/D \gtrsim 3$, see e.g. Bastankhah and Porté-Agel (2017)) accurately for both aligned (Martínez-Tossas et al., 2015) and yaw misalignment wind turbines (Lin and Porté-Agel, 2019). Since the goal of the present study is controller synthesis and sensitivity experiments, more computationally expensive actuator line simulations are left for future work given the large volume of simulations that are run.

Earth's rotational vector is given by $\Omega = [0, \cos(\phi), \sin(\phi)]$, where ϕ is the latitude. The traditional approximation, which neglects the horizontal component of Earth's rotation ~~(Leibovich and Lele, 1985)~~(Leibovich and Lele, 1985; Howland et al., 2018), is not enforced. Therefore, Earth's full rotational vector is included resulting in wind farm dynamics which are sensitive to the direction of the geostrophic wind (Howland et al., 2020b). For simplicity all simulations are performed with west to east geostrophic wind. The Coriolis terms are parameterized by the Rossby number $Ro = G/\omega L$, where G is the geostrophic wind speed magnitude, ω is Earth's angular velocity, and L is the relevant length scale of the problem. All wind speeds used in this study will be normalized by the geostrophic wind speed magnitude. The nondimensional potential temperature is given by θ. The buoyancy term is parameterized by the Froude number $Fr = G/\sqrt{gL}$, where g is the gravitational acceleration. The equation for the transport of the filtered nondimensional potential temperature is given by

$$\frac{\partial \theta}{\partial t} + u_j \frac{\partial \theta}{\partial x_j} = -\frac{\partial q_j^{SGS}}{\partial x_j}, \tag{23}$$

where q_j^{SGS} is the subgrid scale (SGS) heat flux.

The wind is forced by prescribing the geostrophic approximation where the geostrophic pressure gradient drives the mean flow (Hoskins, 1975). The geostrophic pressure balance in the stable free atmosphere is given by

$$\frac{\partial P^G}{\partial x_i} = -\frac{2}{Ro} \varepsilon_{ijk} \Omega_j G_k, \tag{24}$$

with G_k representing the geostrophic velocity vector.

The simulations utilize a fringe region to force the inflow to a desired profile (Nordström et al., 1999). ~~In the uniform inflow cases, the fringe region forces the flow to a uniform profile. In the~~ In the conventionally neutral ABL cases, the concurrent precursor method is applied wherein a separate LES of the ABL is run without wind turbine models and the fringe region is used to force the primary simulation outflow to match the concurrent precursor simulation outflow (see e.g. Munters et al., 2016; Howland et al., 2020a).

~~For the uniform inflow and conventionally neutral cases, there~~ There is an initial startup transience following the domain initialization. ~~The uniform inflow domain is initialized with $u = 1$ in the streamwise direction.~~ Detailed comments on the initialization for the conventionally neutral case are given by Howland et al. (2020b). The simulation cases are run until statistical ~~stationarity and~~ quasi-stationarity is reached~~for the uniform and conventionally neutral cases, respectively~~. The conventionally neutral case is statistically quasi-stationary due to inertial oscillations ~~(see Allaerts and Meyers, 2015, for a detailed discussion on the conv~~ (see Allaerts and Meyers, 2015, for a detailed discussion on the conventionally neutral ABL statistical quasi-stationarity). Upon convergence, the wake steering control strategy is initiated.

The control is initialized with greedy baseline yaw alignment which is fixed for n_T time steps. After n_T simulation steps, with the time averaged power production for each wind turbine measured over the previous ~~$n_T - 2T_a$~~ $n_T - T_a$ time steps, ~~the~~ with the advection time scale given by T_a, the EnKF state estimation and optimal yaw calculations are performed (Figure 1). The time-lag associated with the advection time scale of the wind farm is estimated by invoking Taylor's hypothesis (see Appendix C for a brief discussion). The yaw angles are then implemented and held fixed for n_T time steps and the cycle repeats. The wind speed, wind direction, and power production are averaged in time over the window. The state estimation and yaw misalignment update steps are performed concurrently with a period of n_T simulation steps. In general, these two processes can be decoupled, although this was not investigated in the present study. Typical utility-scale wind turbines have a yaw rate of approximately $0.5°/s$ (Kim and Dalhoff, 2014). For the largest yaw misalignment change in one control update step in this study of approximately $30°$, when the wake steering control is initialized, the yawing action is completed in approximately one minute, which is significantly less than the advection timescale in the flow. Therefore, the yaw rate will not influence the results presented in this study.

In order to compare the power production of the yaw misalignment control strategy with the baseline greedy control, a separate LES case is run for each experiment with yaw aligned control. The two simulations are initialized from identical domain realizations and the computational timestep Δt is fixed between the two cases. Therefore, without the influence of variable turbine operation, the flow within and around the turbine array is identical to machine precision between the two yaw aligned and yaw misaligned cases[2]. Since this study will consider the conventionally neutral ABL which contains turbulence and inertial oscillations, this separate simulation must be used instead of a comparison with the power production of the first yaw control update step (see Appendix B).

~~4 Dynamic wake steering uniform inflow LES~~

~~In this section, the dynamic closed-loop wake steering controller described by Figure 1 will be used in LES of two turbines operating in uniform inflow. The domain has lengths of $25D$, $10D$, and $10D$ in the x, y, and z directions, respectively, and the number of grid points are 128, 64, and 64. Two actuator disk model wind turbines are simulated in uniform inflow with slip walls on all sides and a fringe region at the domain exit to force the inflow to a uniform profile. The fringe is used in the last 25% of the computational x domain. The turbines are located $4D$ apart in the streamwise direction and are misaligned by $0.25D$ in the spanwise direction as shown in Figure F1. Due to the spanwise misalignment, the preferential yaw misalignment direction for the upwind turbine is positive (counter-clockwise rotation viewed from above).~~

~~The flow is stationary after the initial startup transient has decayed and therefore the optimal yaw misalignment angles for the two wind turbines are not a function of time. The flow is initialized as described in Section 3. Upon statistical stationarity, the closed-loop wake steering controller is initialized and the flow is run for $n_T = 10000$ LES time steps to ensure sufficient~~

[2] In chaotic dynamical systems, differences caused by changes in the compiler optimization will grow exponentially in time (Senoner et al., 2008). We have ensured that these floating-point differences are eliminated by fixing compiler optimization and processor topology to allow for quantitative, temporal comparisons between the LES cases. The results are therefore repeatable to machine precision.

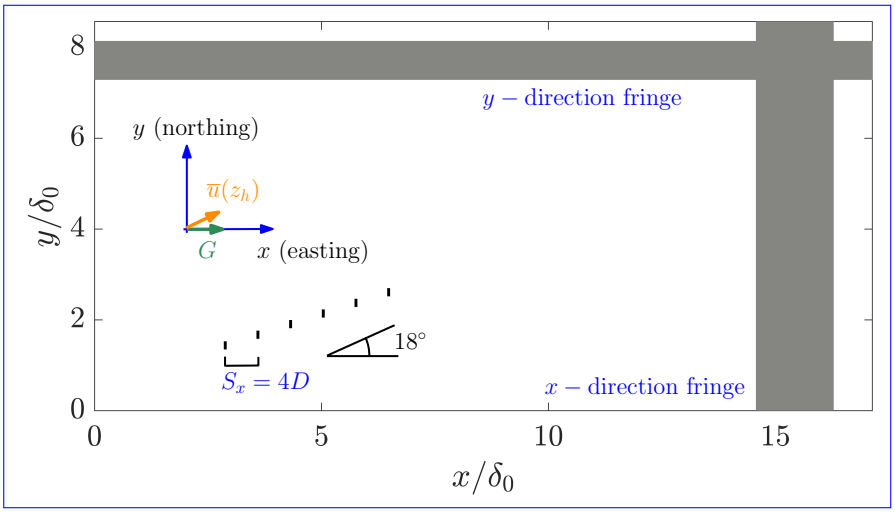

Figure 3. ~~Uniform inflow LES~~ Conventionally neutral six wind turbine finite wind farm simulation ~~actuator disk model layout~~setup. The ~~fringe region~~ geostrophic wind direction is ~~represented by the dashed black line~~ west to east and the x-axis is aligned with the geostrophic wind ~~turbines are shown~~ direction. The mean wind direction at hub height, $\tan^{-1}(\overline{v}/\overline{u}) \approx 16^\circ$ but is not known *a priori* in the simulation and varies as ~~solid black lines~~a function of time. The wind turbine array is offset from alignment in the x-direction by 18°. The initial boundary layer height δ_0 is 700 meters and does not change significantly during runtime (see Figure 4). Fringe functions are applied in the x and y directions to establish a finite wind farm simulation.

~~averaging. The time averaging is initialized following the advection time of the wind farm (see Section C) and therefore there are $n_T - 2T_a$ timesteps within each time averaging window.~~ wind turbines have a rotor diameter of 126 meters and a hub height of 100 meters. The thrust coefficient is $C_T = 0.75$. The initial boundary layer height is 700 meters. The domain size is $12 \times 6 \times 2.4$ kilometers in the x, y, and z directions, respectively, with z representing the wall-normal coordinate. The number of grid points is $480 \times 240 \times 192$ with a grid spacing of $25\text{m} \times 25\text{m} \times 12.5\text{m}$. The grid spacing is uniform and the mesh size is similar to previous studies (Allaerts and Meyers, 2015) and a grid convergence study was performed by (Howland et al., 2020b) for the conventionally neutral ABL. Six model wind turbines are incorporated in the domain and the layout within the computational domain is shown in Figure 3. The Rossby number based on the wind turbine diameter is 544 and the Froude number is 0.14. The vertical profiles of velocity, potential temperature, and streamwise turbulence intensity for the precursor simulation for two domain snapshots are shown in Figure 4.

4 Dynamic wake steering conventionally neutral atmospheric boundary layer LES

In this section, we will utilize the closed-loop wake steering controller ~~that was validated in Section F for uniform inflow in~~ in the conventionally neutral ABL. While the conventionally neutral ABL is statistically quasi-stationary, the optimal yaw misalignment angles will vary as a function of time due to turbulence, large-scale streamwise structures (Önder and Meyers, 2018),

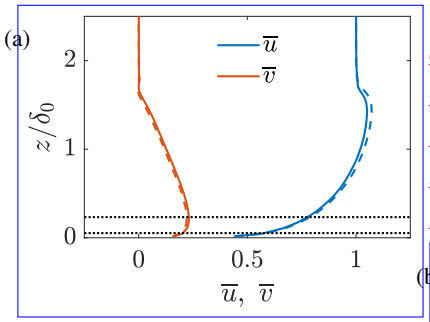

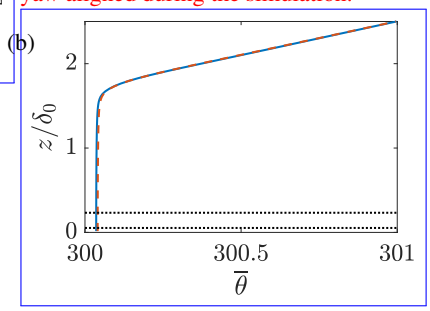

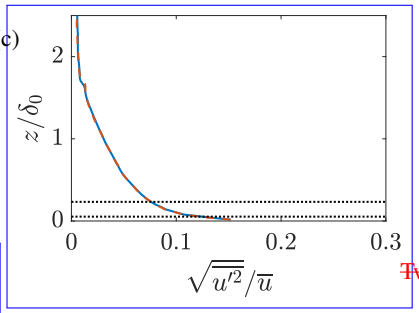

Two wind turbine model uniform inflow LES (a) power production. (b) The yaw misalignment angle γ for the upwind turbine. The downwind turbine remains yaw aligned during the simulation. Two wind turbine model uniform inflow LES (a) k_w and σ_0 for the upwind turbine and (b) $\hat{P}$ and P for the downwind turbine.

The sum of power production for the two turbine pair as a function of the control update steps is shown in Figure F2(a). The power production is normalized by the greedy control simulation. The power production for the first yaw controller update time step is equal to 1 since yaw misalignment has not been implemented and the model is gathering power production data to be used for the first EnKF data assimilation pass. The power production increases in the second time step when yaw misalignment in incorporated for the upwind turbine (Figure F2(b)). The controller correctly commands the upwind turbine to positive yaw misalignment. While the flow is stationary, the upwind turbine yaw misalignment angle changes marginally after the second time step. These changes can be attributed to modifications to the wake model parameters as a function of time as estimated by the EnKF (Figure F3(a)). The estimated model parameters vary in time in this stationary flow due to standard error of the mean with limited samples within a given time window of length T, due to the influence of the yaw misalignment of the dynamics on the wake, and due to the limited number of ensembles N_e in the EnKF.

The wake model parameters have a functional dependence on the yaw misalignment of the turbines within the wind farm. The wake of a yaw misaligned turbine is narrower than the same turbine when yaw aligned (Archer and Vasel-Be-Hagh, 2019). The wake spreading rate k_w dictates the wake recovery rate. Yaw misalignment also reduces the axial induction factor of the wind turbine and therefore affects the wake recovery. Further, since wind turbines in yaw misalignment generate large-scale counter rotating vortices (Howland et al., 2016), the wake recovery rate will likely be enhanced in yaw misalignment (Fleming et al., 2018). As a result of these vortices, the wake will have top-down asymmetry and this will influence σ_0. While the present model neglects the vertical dimension, the development of a controls-oriented model which incorporates the curled wake asymmetry is ongoing (Martínez-Tossas et al., 2019). Future work should characterize the influence of yaw misalignment on the wake spreading rate.

The state-estimated power production for the downwind turbine is compared to the LES power production in Figure F3(b). The downwind turbine's power production in the greedy control strategy is low (approximately $0.2P_1$) due to the freestream inflow condition and close streamwise direction spacing. The EnKF results in an accurate power production estimation using the lifting line model. While the wake model parameters are changing as a function of time (Figure F3(a)), the power production estimate for the downwind turbine is not significantly affected. The wake model parameters k_w and σ_0 are anti-correlated as a function of time. Within the two-parameter lifting line model, increasing k_w or σ_0 reduces the wake effect for the downwind turbine. With the LES power production of the downwind turbine and the yaw misalignment of the upwind turbine approximately fixed, the state estimation increases one parameter and reduces the other parameter to remain consistent in the estimation of the downwind power. This indicates, similarly to the results in Appendix A, that the two parameter lifting line model may be overparameterized which may lead to overfitting. The accuracy of the EnKF state estimation and lifting line model in the prediction of the power production in yaw misalignment will be tested in Section 4. This accuracy will implicitly measure the impact of overfitting in the model. Since there is no wake impinging on the upwind turbine , the state estimation has no impact on the

and inertial oscillations. A suite of LES cases is run to test the influence of the controller architecture design, state estimation design, P_p estimate (Eq. 6), and the wind farm layout on the power production increases over greedy baseline operation as a result of wake steering control. Each sensitivity study represents a new LES case which is run using the concurrent precursor methodology described in Section 3.

All quasi-steady conventionally neutral ABL simulations have a yaw controller update of $n_T = 1000$ time steps which approximately equal to $\tau = 3000$ seconds or 50 minutes. The advection time scale from the first to the last wind turbine in the array is approximately 9 minutes and the time lag is taken as two times the approximate advection time scale based on Taylor's Hypothesis. Therefore, each update contains approximately 30 minutes of statistical averaging, or about 600 time steps. The long time averaging window was selected since the flow is statistically quasi-stationary and to ensure temporal averages with reduced noise. In transitioning ABL environments, the time averaging window should likely be reduced (Kanev, 2020). The greedy baseline controller yaw alignment is updated according to the same timescales based on the mean wind direction measured locally by each wind turbine. The nacelle position for the yaw misaligned turbines is based on the wind direction measurement at each local turbine as well as the controller estimated optimal yaw misalignment angles, i.e. $n_\alpha = \alpha + \gamma$ where n_α is the nacelle position and α is the wind direction incident to the wind turbine.

~~The wind turbines have a rotor diameter of 126 meters and a hub height of 100 meters (selections based on NREL 5 MW turbine, Jonkma . The thrust coefficient is $C_T = 0.75$. The initial boundary layer height is 700 meters. The domain size is $12 \times 6 \times 2.4$ kilometers in the x, y, and z directions, respectively, with z representing the wall-normal coordinate. The number of grid points is $480 \times 240 \times 192$ with a grid spacing of $25\text{m} \times 25\text{m} \times 12.5\text{m}$. The grid spacing is uniform and the mesh size is similar to previous studies (Allaerts and Meyers, 2015) and a grid convergence study was performed by (Howland et al., 2020b) for the conventionally neutral ABL. Six model wind turbines are incorporated in the domain and the layout within the computational domain is shown in Figure 3. The Rossby number based on the wind turbine diameter is 544 and the Froude number is 0.14. The vertical profiles of velocity, potential temperature, and streamwise turbulence intensity for the precursor simulation for two domain snapshots are shown in Figure 4.~~

~~Conventionally neutral six wind turbine finite wind farm simulation setup. The geostrophic wind direction is west to east and the x-axis is aligned with the geostrophic wind direction. The mean wind direction at hub height, $\tan^{-1}(\overline{v}/\overline{u}) \approx 16°$ but is not known a prioriin the simulation and varies as a function of time. The wind turbine array is offset from alignment in the x-direction by $18°$. The initial boundary layer height δ_0 is 700 meters and does not change significantly during runtime (see Figure 4). Fringe functions are applied in the x and y directions to establish a finite wind farm simulation.~~

~~Horizontally averaged concurrent precursor conventionally neutral ABL LES (a) velocity, (b) potential temperature, and (c) turbulence intensity. Two different instantaneous domain snapshots are shown in solid (early) and dashed (late) lines. Dashed-dotted lines show the extents of the turbine rotor area.~~

This section is organized as follows: Section 4.1 examines the sensitivity of the wind turbine array power production to the wake steering controller design. Section 4.2 tests the sensitivity to the state estimation methodology. The sensitivity of the wake steering control to the estimate of P_p is discussed in Section 4.3. The accuracy of the wake model power predictions

Case	Steering	Static yaw	Static k_w, σ_0	Advection	Feedforward k_w, σ_0	~~P_p~~ $\hat{P}_p$	$\frac{\sum P - \sum P_{\text{aligned}}}{\sum P_{\text{aligned}}}$ (%)	$\overline{\sum P} \pm \text{STD}(\sum P)$
	Wind turbine column alignment 18°							
NA	-	-	-	✓	-	3	-	3.01 ± 0.13
NL	✓	✓	✓	✓	-	3	5.4	3.17 ± 0.14
ND1	✓	-	-	✓	~~-~~ ✓	3	~~0.2~~ 4.6	~~3.01 ± 0.12~~ 3.15 ± 0.1
ND2	✓	-	-	✓	-	3	~~4.6~~ 0.2	~~3.15 ± 0.14~~ 3.01 ± 0.1
ND3	✓	-	✓	✓	-	3	5.7	3.18 ± 0.13
~~ND4~~ NDP2	✓	-	-	✓	✓	2	-3.0	2.92 ± 0.13
~~ND5~~ NDP4	✓	-	-	✓	✓	4	5.1	3.16 ± 0.16
ND6	✓	-	-	-	✓	3	4.2	3.13 ± 0.12
	Wind turbine column alignment 14°							
NA14	-	-	-	✓	-	3	-	2.96 ± 0.09
ND141	✓	-	-	✓	✓	3	1.1	2.99 ± 0.10
ND142	✓	-	✓	✓	-	3	1.0	2.99 ± 0.11

Table 1. The conventionally neutral finite wind farm wake steering cases. The mean power production increase with respect to yaw aligned operation is calculated over approximately 24 hours of physical wind farm operation. Case NA is yaw aligned wind farm operation. Case NL approximates open-loop lookup table based control. Cases beginning with ND are dynamic, closed-loop control cases with various control architectures as denoted in the table. The wake model estimate for P_p is $\hat{P}_p$.

is discussed in Section 4.4. ~~Finally, Section~~ Appendix E characterizes the influence of the wind farm alignment on the wake steering power production increase. ~~The conventionally neutral ABL wake steering results are summarized in Table 1.~~

The conventionally neutral ABL wake steering LES cases and results are summarized in Table 1. Baseline yaw aligned wind turbine operation is given by Case NA, where the yaw alignment is updated at the same temporal frequency as the dynamic yaw control is updated to ensure quantitative comparisons as a function of time. Case NL approximates open-loop lookup table operation, where the yaw misalignment is prescribed as a function of the incident wind speed and direction rather than dynamically adapting to the local inflow conditions. Cases ND1, ND2, and ND3 use dynamic wake steering control with varying parameter estimation techniques. In Case ND1 the wake model parameters are optimized continuously based on a fixed parameter initialization. Cases ND1 and NL are discussed in detail in §4.1. In Case ND2, the model parameters are optimized continuously in time based on an initialization using the previous time step optimal parameters, and finally Case ND3 fixes the wake model parameters after the estimation in the first control update step. The influence of the state estimation techniques are discussed in detail in §4.2. Cases NDP2 and NDP4 modify the wake model estimate for P_p and are described in more detail in §4.3. Finally, Case ND6 is the same as Case ND1 except it sets the advection time $T_a = 0$. Cases NA14, ND141, and ND142 modify the wind farm alignment to 14° with respect to the horizontal axis and are described in more detail in Appendix E.

The statistical significance of the array power productions for the various wake steering cases with respect to baseline control Case NA are shown in Figure 5. The statistical significance is characterized with one-sided two-sample Kolmogorov-Smirnov

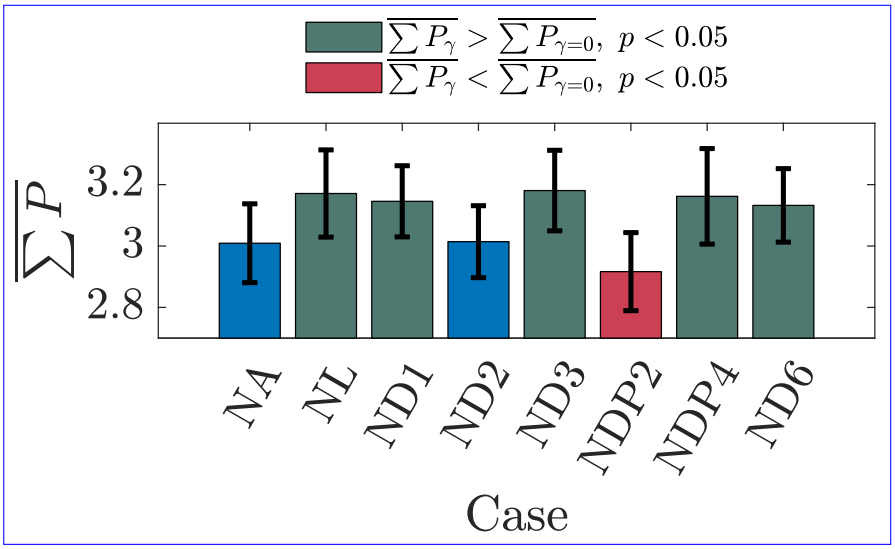

Figure 5. Time averaged sum of the six turbine array power production for the conventionally neutral ABL LES cases described in Table 1. The errorbars denote one standard deviation in the power production. The power production is normalized by the leading turbine P_1 in baseline control conditions. The statistical significance of the wake steering power production difference with respect to baseline control Case NA are indicated by the colors. The statistical significance is characterized by a one-sided two-sample Kolmogorov-Smirnov test at a 5% significance level. Case NA is blue and Case ND2 does not have statistically significantly greater power production than Case NA. Green cases have statistically significantly ($p < 0.05$) more power than Case NA. Red cases have statistically significantly ($p < 0.05$) less power than Case NA.

tests for the given case with respect to baseline control Case NA at a 5% significance level. The Kolmogorov-Smirnov test was selected since it does not enforce a normal distribution assumption on the data. Cases NL, ND1, ND3, NDP4, and ND6 produce significantly more power than baseline control Case NA. Case NDP2 produces significantly less power than baseline control and Case ND2 is not significantly different than Case NA. None of the Cases NL, ND1, ND3, NDP4, and ND6 are significantly different from each other. The power production for each turbine for each wake steering case is shown in Figure 6.

4.1 Comparison between dynamic and quasi-static wake steering approaches

The dynamic wake steering controller described in Figure 1 is compared to lookup table static control in this section. Since the flow is statistically quasi-stationary, the mean wind speed and direction at hub height do not change significantly as a function of time. Therefore, during simulation, the flow remains at wind conditions which would be associated with one wind speed and direction bin in tabulated lookup table wake steering control. The lookup table control is approximated by fixing the yaw misalignment angles as a function of time after the initial optimal angles are computed during the first yaw controller update (Case NL). Numerical experiments (not shown for brevity) demonstrated that modifying the control update step from which

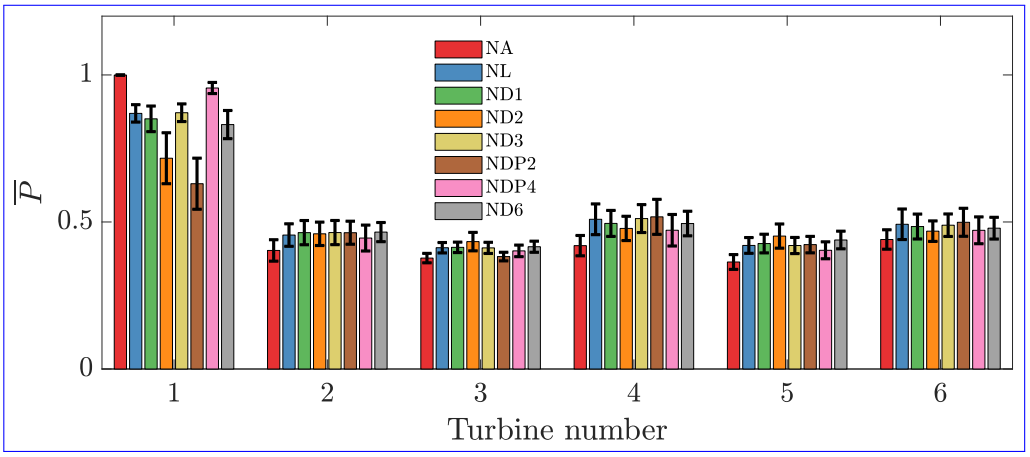

Figure 6. Time averaged power production for each turbine in each wake steering case. The errorbars denote one standard deviation in the power production. The power production is normalized by the leading turbine P_1 in baseline control conditions.

the lookup yaw misalignment values were computed did not have a statistically significant influence on the results for Case NL. The dynamic yaw controller is represented by Case ~~ND2.~~ ND1. The time averaged wind speed at the wind turbine hub height for Cases NA and NL are shown in Figure 7. As a result of the positive yaw misalignment strategy in Case NL (Figure 7(b)), the individual and collective array wakes are deflected in the clockwise direction compared to the aligned configuration of Case NA (Figure 7(a)).

The yaw misalignment angles as a function of the yaw controller updates for Cases NL and ~~ND2~~ ND1 are shown in Figure 8. The yaw angles in this study are defined as the misalignment with respect to the local inflow direction incident on the particular turbine in the array. While the lifting line model does not explicitly incorporate the effects of secondary steering for which model development is on-going (see e.g. King et al., 2020), the model selects yaw misalignment angles which are large for the first turbine and generally decrease further into the wind farm, which is consistent with the optimal values found by recent wind tunnel experiments (Bastankhah and Porté-Agel, 2019). Since the flow is statistically quasi-stationary, the dynamic algorithm yaw misalignment angles do not change significantly as a function of time. There are a few yaw misalignment changes on the order of $10°$ during one yaw update. ~~The change in yaw misalignment in a single control update is not limited explicitly in this study. The~~ The time averaged power productions as a function of the yaw controller updates for the two cases are shown in Figure 9. The qualitative trends in power production are similar between the two cases. Quantitatively, the lookup table static yaw misalignment Case NL increased the power production 5.4% with respect to the baseline greedy control while the dynamic yaw Case ~~ND2~~ ND1 increased the power by 4.6%.

The quantitative influence of wake steering is a function of the layout and ABL conditions. As the focus of the present study is assessing the sensitivity of wake steering to controller architecture, model parameters, and wind farm layout, measures of the statistical significance of the results are useful. However, the statistical significance of the results (e.g. whether Case NL significantly outperformed Case ~~ND2~~ND1) does not indicate, necessarily, that lookup table control is better than the dynamic

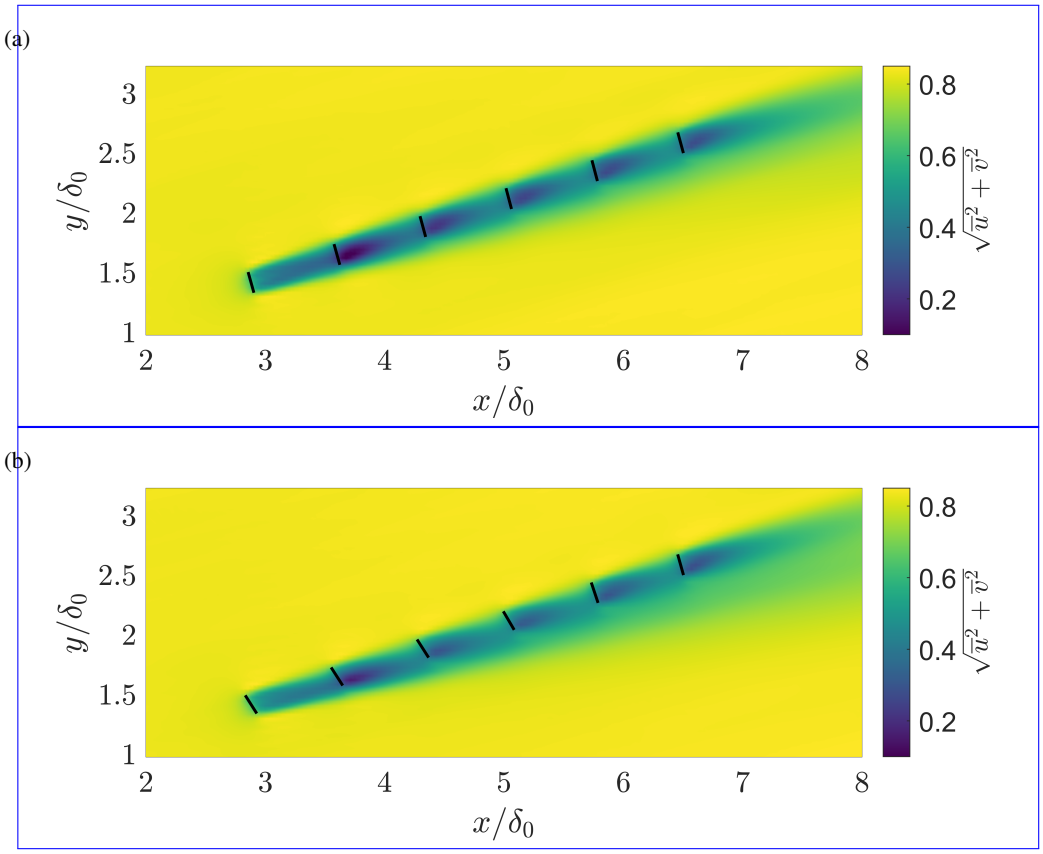

Figure 7. Time averaged wind speed $\sqrt{\overline{u}^2+\overline{v}^2}$ at the wind turbine hub height of $z = 100$ meters for (a) baseline yaw aligned control Case NA and (b) wake steering control Case NL. The wind turbines are shown with black lines. The yaw misalignment values for Case NL are shown in Figure 8.

controller used in Case ~~ND2~~ ND1 for all wake steering applications but rather, that it was better for the specific ABL setup and computational time window of the experiment. ~~In this study, we will consider a control case to be significantly superior to another if the mean array power production averaged over the control update steps is more than one standard deviation larger than the other case. The mean and standard deviations of the array power productions over the control update steps~~ The statistical significance of the power production increase with respect to baseline control Case NA are shown in ~~Table 1.~~ Figure 5. Cases NL and ~~ND2~~ ND1 have significantly higher power than Case NA but the power in Case NL is not significantly higher than in Case ~~ND2~~ND1.

~~Although it is not significant, there are several possible reasons for the static yaw misalignment's slightly superior performance compared to the dynamic yaw controller. The yaw selection may overfit to the previous time window and select angles which are suboptimal for the next time window (tested further in Section 4.2). The~~ The relationship between the wake model power prediction and the measured LES power production is shown for the two cases in Figure 10. The wake model overpredicts the

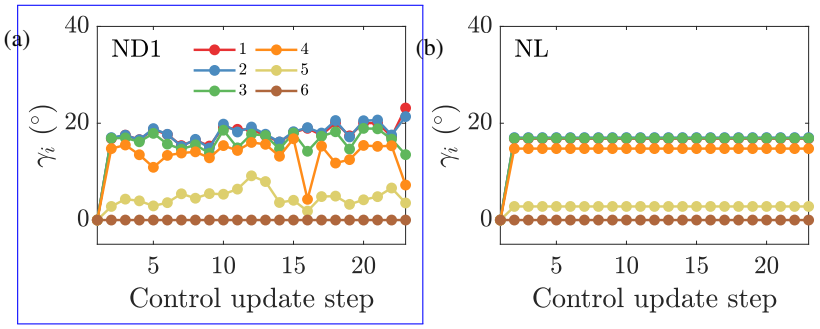

Figure 8. Wind farm yaw misalignment angles γ_i for each turbine for (a) online control using the initial parameters to initialize the next state (~~ND2~~ND1) and (b) and the lookup table control (NL).

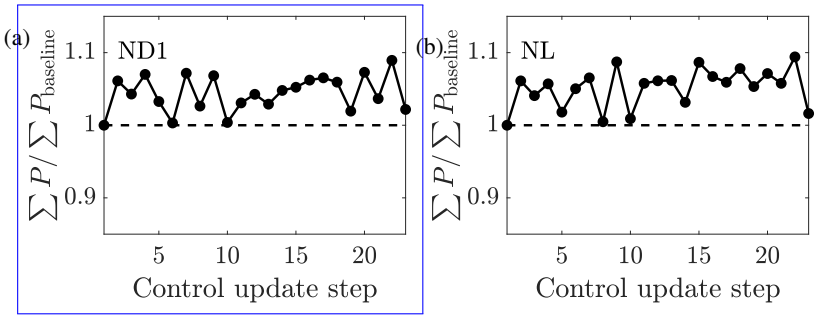

Figure 9. Time averaged wind farm power production as a function of the control update steps for (a) online control using the initial parameters to initialize the next state (~~ND2~~ND1) and (b) and the lookup table control (NL). The wind farm power is normalized by the power production of the aligned wind farm case.

power production in yaw misalignment more for the dynamic yaw control than the lookup table control. After the first time step, the wake model no longer has any state information for the LES power production with greedy baseline control since the previous state had yaw misalignment. When the wake model overpredicts the expected LES power, the wake model parameters are updated to a state which expects larger wake loss effects in baseline control; therefore, the yaw misalignment angles are increased at the next time step. The yaw misalignment angles for the leading turbine oscillate around the lookup table optimal forecast which was based on calibration with power data from greedy baseline control alone (Figure 8). The dynamic yaw increased power slightly less than the static yaw misalignment case, but not significantly less. However, eliminating the need to tabulate historical data and the complexity of implementing a lookup table-based controller could be beneficial in a practical controller setting. Further, the conventionally neutral boundary layer does not occur often in practice (Hess, 2004). Therefore, in a practical setting, the wind direction and speed at hub height will not be fixed for multiple hours as in this test problem.

In Case ND6, the power productions are time averaged over the full n_T window without considering the advection time scale in the controller design. The power production increase over greedy control is 4.2% in this case which is less than the 4.6%

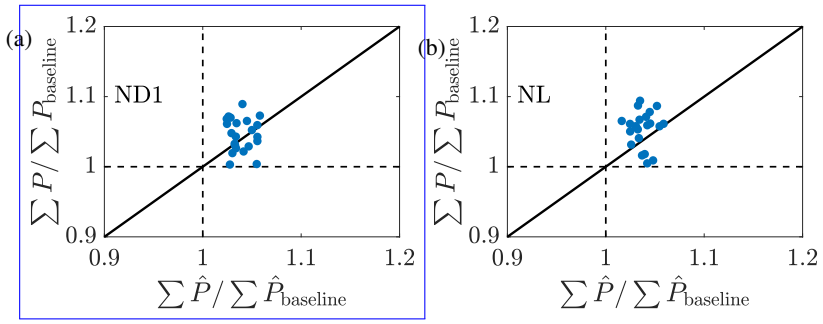

Figure 10. Relationship between the LES wind farm power production compared to the wake model wind farm power production prediction for (a) online control using the initial parameters to initialize the next state (ND1) and (b) and the lookup table control (NL). The wind farm power is normalized by the power production of the aligned wind farm case. The LES power production is given by P and the wake model prediction is given by $\hat{P}$.

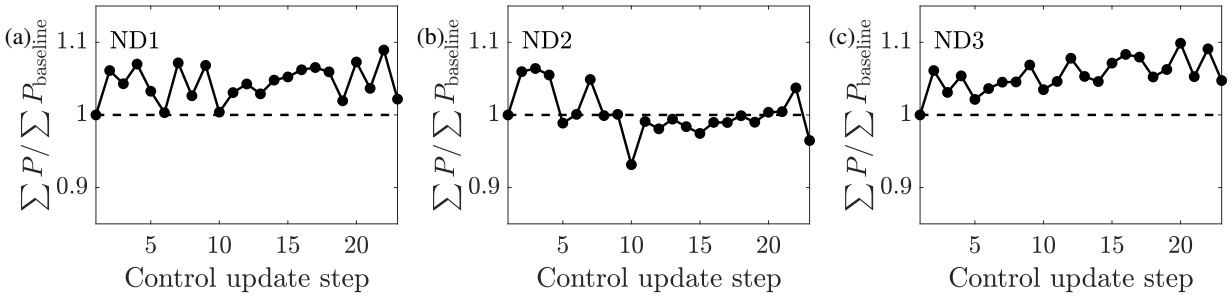

Figure 11. Time averaged wind farm power production as a function of the control update steps for (a) online control using the ~~previous optimal~~ initial parameters to initialize the next state (ND1), (b) online control using the ~~initial~~ previous optimal parameters to initialize the next state (ND2), and (c) and the static state estimation control (ND3). The wind farm power is normalized by the power production of the aligned wind farm case.

increase when considering the advection time lag (Case ~~ND2~~ND1), although this difference is not significant. The dynamics of the closed-loop controller over long experimental horizons are tested in a 50 control update simulation in Appendix D.

4.2 Influence of the state estimation

The influence of the state estimation methodology is tested in this section. Within the conventionally neutral ABL, three experiments are run, focused on the state estimation initialization. ~~In~~ The initial model parameters in the EnKF state estimation are held fixed at $k_w = 0.1$ and $\sigma_0 = 0.25$ in Case ND1. In Case ND2, the optimal EnKF estimated parameters from the previous time step are used to initialize the state estimation of the current time step. ~~The initial model parameters are held fixed at $k_w = 0.1$ and $\sigma_0 = 0.25$ in Case ND2.~~ Finally, Case ND3 fixes the model parameters after the first time step. Case ND3 differs from Case NL from Section 4.1 since the optimal yaw misalignment angles may vary as a function of time while the model parameters do not.

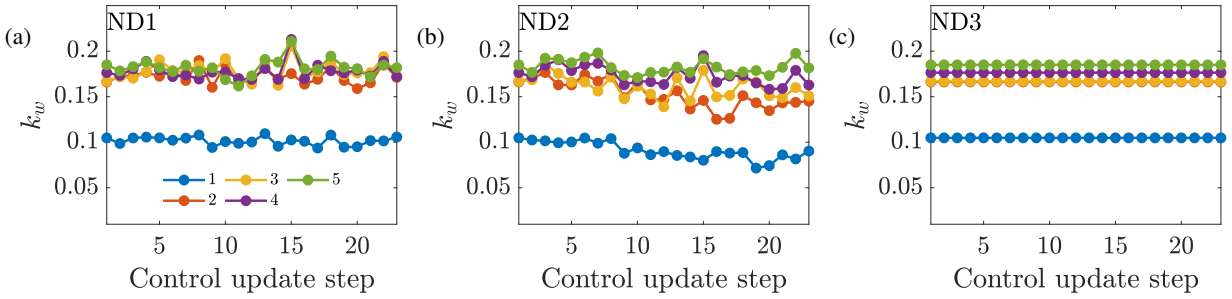

Figure 12. Wake spreading coefficient for each turbine in the wind farm for (a) online control using the ~~previous optimal~~ initial parameters to initialize the next state (ND1), (b) online control using the ~~initial~~ previous optimal parameters to initialize the next state (ND2), and (c) and the static state estimation control (ND3).

The power productions as a function of the yaw controller update for the three cases are shown in Figure 11. Case ~~ND1~~ ND2 has significantly less power production than Cases ~~ND2~~ ND1 and ND3. The time averaged power production increases with respect to the baseline, greedy control is ~~0.2%,~~ 4.6%, 0.2%, and 5.7% for cases ND1, ND2, and ND3, respectively. The power production in Cases ~~ND2~~ ND1 and ND3 are significantly higher than Case NA while Case ~~ND1~~ ND2 is not. Further, Cases ~~ND2~~ ND1 and ND3 are significantly better than ~~ND1~~ ND2 but Case ND3 is not significantly better than ~~ND2~~ND1. In the EnKF methodology described in Section 2.2, the update step to the wake parameters is limited by the imposed parameter variance (σ_{k_w} and σ_{σ_0}). Therefore, the initialization of the EnKF with fixed parameters limits the perturbation of the estimated parameters as a function of time whereas the initialization with the previous optimal parameters allows k_w and σ_0 to vary more significantly over time. The EnKF estimated k_w and σ_0 for the three cases are shown in Figures 12 and 13, respectively. While the proportionality constant σ_0 of the presumed Gaussian wake does not have a clear trend for Case ~~ND1~~ND2, the estimated wake spreading rate k_w is clearly decreasing for all wind turbines as a function of time. For Case ~~ND2~~ND1, the estimated model parameters do not have a clear trend and remain approximately constant as a function of time. As the estimated wake spreading rate is decreased, the wake model predicts worsening wake interactions and lower array power production given greedy baseline control. As a result, the model predicted optimal yaw misalignment angles increase as a function of time for Case ~~ND1~~ ND2 as shown in Figure 14(a). While Cases ~~ND2~~ ND1 and ND3 predict the optimal yaw misalignment for the most upwind turbine to be approximately 20°, and decreasing γ moving downwind, Case ~~ND1~~ ND2 increases the yaw misalignment for the upwind turbine to as high as 30°. ~~While this case was not run further, it is not expected that this trend would continue unboundedly with controller instability since the power production penalty as a function of increased yaw misalignment is significant beyond 40°. The typical yaw rate for utility-scale horizontal axis wind turbines is around 0.5 degrees per second. For the largest discrete yaw misalignment change in the present study of $\approx 30°$ (Figure 14(a)), the yaw misalignment change would take ≈ 75 seconds. This time is significantly less than the advection time T_a, and is therefore does not impact the control system and power production results here.~~

The relationship between the model predicted and LES measured power production for the three cases is shown in Figure 15. Case ~~ND1~~ ND2 has an increased occurrence of wake model over-prediction of the power production while Case ND3 has

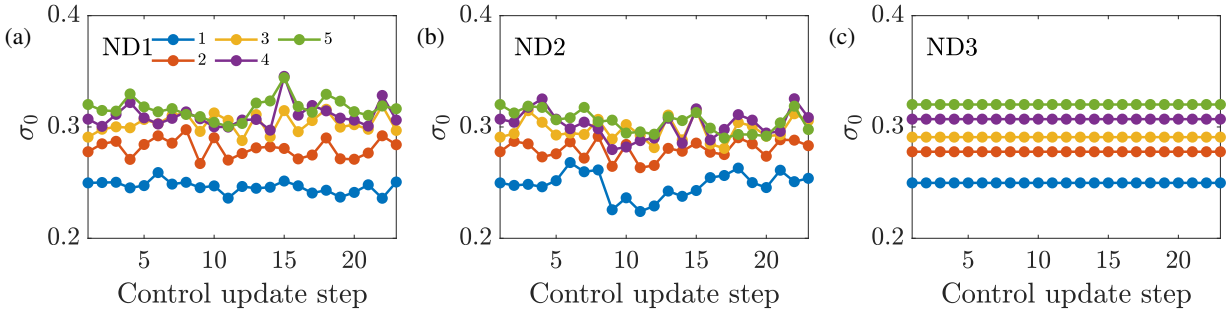

Figure 13. Proportionality constant for the presumed Gaussian wake for each turbine in the wind farm for (a) online control using the ~~previous optimal~~ initial parameters to initialize the next state (ND1), (b) online control using the ~~initial~~ previous optimal parameters to initialize the next state (ND2), and (c) and the static state estimation control (ND3).

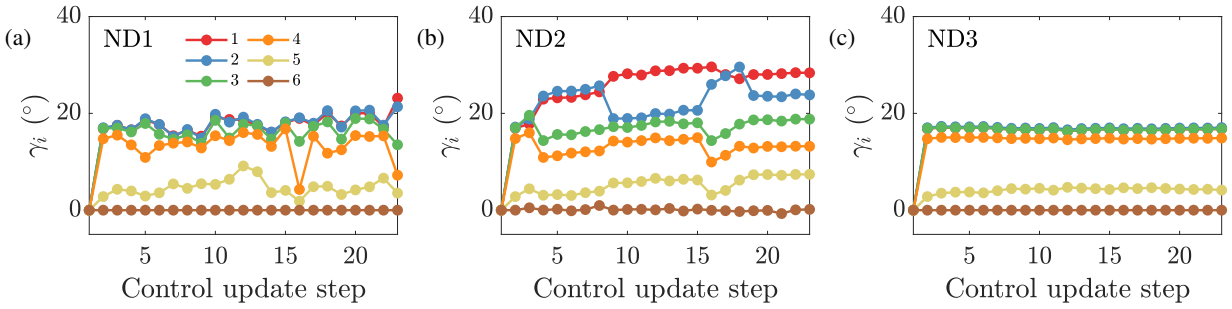

Figure 14. Yaw misalignment angles for each turbine in the wind farm for (a) online control using the ~~previous optimal~~ initial parameters to initialize the next state (ND1), (b) online control using the ~~initial~~ previous optimal parameters to initialize the next state (ND2), and (c) and the static state estimation control (ND3).

an increased occurrence of wake model under-prediction. Case ~~ND2~~ ND1 has approximately equal occurrence of under- and over- prediction. The efficacy of the state estimation is shown in Figure 16. Both Cases ND1 and ND2 are able to estimate the power production for the downwind turbine in the baseline, greedy operation (the first time step) and with yaw misalignment. Since Case ND3 uses static state estimation, there are some discrepancies between the LES power production and the lifting line model (Figure 16(c)). The power production for the most upwind turbine is modeled accurately using $P_p = 3$, although the LES power production is generally slightly lower, indicating $P_p > 3$ for this ADM and ABL state.

The most successful dynamic control framework utilized in the conventionally neutral ABL is the static state estimation methodology (Case ND3), although the differences between Cases ND1 (parameter estimation from standard initialization), ND3 (static parameters after first control step), and NL (static yaw angles after first control step) are not significant. While the optimal yaw misalignment angles change slightly as a function of time (Figure 14), the wake model parameters are fixed. Since the flow is statistically quasi-stationary, the wake model parameters should not change significantly as a function of time. However, the wake model parameters may have a ~~function~~ functional dependence on γ, the yaw misalignment for the upwind

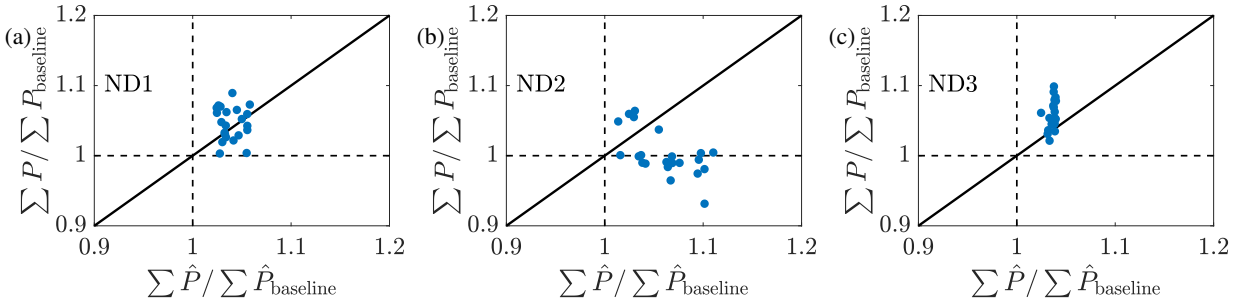

Figure 15. Relationship between the LES wind farm power production compared to the wake model wind farm power production prediction for (a) online control using the ~~previous optimal~~ initial parameters to initialize the next state (ND1), (b) online control using the ~~initial~~ previous optimal parameters to initialize the next state (ND2), and (c) and the static state estimation control (ND3). The LES power production is given by P and the wake model prediction is given by $\hat{P}$.

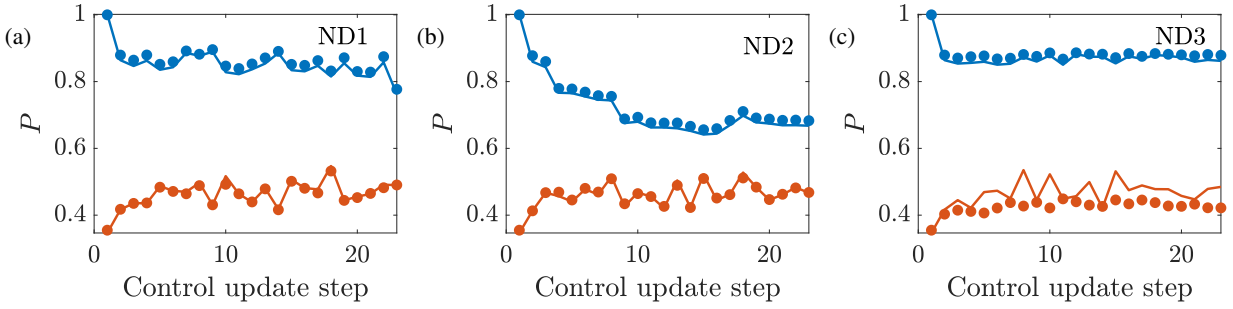

Figure 16. Time averaged power production for the first and second wind turbines in the wind farm as a function of the control update steps for (a) online control using the ~~previous optimal~~ initial parameters to initialize the next state (ND1), (b) online control using the ~~initial~~ previous optimal parameters to initialize the next state (ND2), and (c) and the static state estimation control (ND3). The LES power production is given by P and the wake model state estimation is given by $\hat{P}$.

turbines. This potential dependence of k_w and σ_0 on yaw misalignment was not incorporated explicitly in the present modeling framework, although it is incorporated implicitly through the state estimation, and is recommended for future work.

The static state estimation with dynamic yaw controller is able to outperform the lookup table control (Table 1). This indicates that while the wake model parameters are fixed, the optimal yaw misalignment angles differ even with changes to the mean wind direction less than $1°$. As such, the lookup table based yaw misalignment strategy is unlikely to be optimal in a general setting since it relies on wind speed and direction bins of arbitrary size. Instead, in a lookup table approach, the wake model parameters could be tabulated instead of the optimal yaw misalignment angles. Optimal yaw misalignments can be calculated dynamically, on-the-fly using the computationally efficient model described in Section 2.1 or a mid-fidelity model (e.g. WFSim, Boersma et al., 2018) could be used to compute discrete yaw angles in wind condition bins and the continuous optimal yaw function could be approximated using interpolating functions or a neural network, for example.

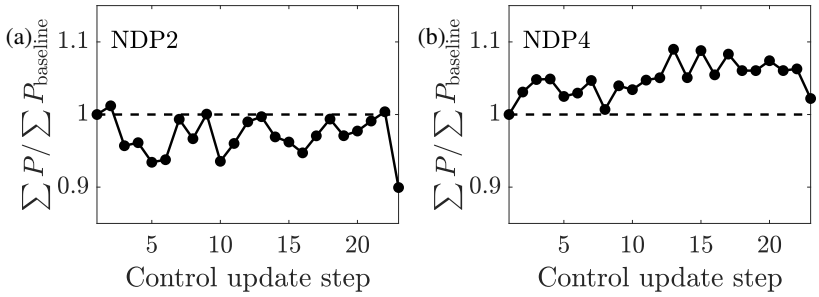

Figure 17. Time averaged wind farm power production as a function of the control update step for online control using the initial parameters to initialize the next state and (a) ~~$P_p = 2$~~ $\hat{P}_p = 2$ (~~ND4~~NDP2) and (b) ~~$P_p = 4$~~ $\hat{P}_p = 4$ (~~ND5~~NDP4). The wind farm power is normalized by the power production of the aligned wind farm case.

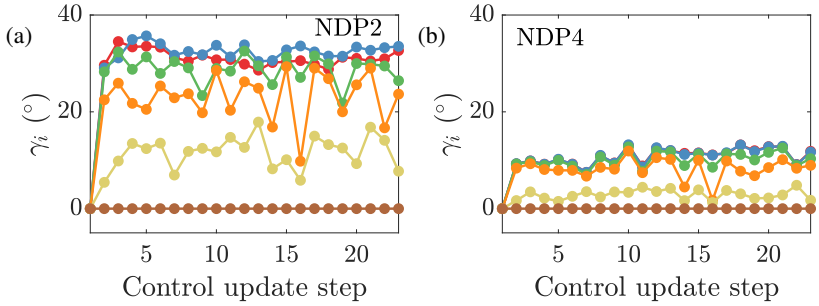

Figure 18. Yaw misalignment angles for each turbine in the wind farm for online control using the initial parameters to initialize the next state and (a) ~~$P_p = 2$~~ $\hat{P}_p = 2$ (~~ND4~~NDP2) and (b) ~~$P_p = 4$~~ $\hat{P}_p = 4$ (~~ND5~~NDP4).

4.3 Influence of the estimate of P_p in the wake model

The wind turbine power production as a function of the yaw misalignment in the wake model is given by Eq. 6. The parameter P_p is uncertain. Following actuator disk theory, ~~$P_p = 3$~~ $P_p \approx 3$, although experiments typically show $P_p \leq 2$ for wind turbines and wind turbine models with rotation (e.g. Medici, 2005). With the ADM used presently, $P_p = 3$ should be an accurate approximation but will be imperfect since actuator disk theory applies only to ~~one dimensional~~spatially uniform, steady flow. Since P_p is wind turbine and likely site-specific, ~~it is likely~~ in a wake steering application~~that~~, the precise value of P_p is generally unknown *a priori*. In this section, we will model P_p as ~~2 (ND4) and 4 (ND5~~ $\hat{P}_p = 2$ (NDP2) and $\hat{P}_p = 4$ (NDP4) using the same control architecture as Case ~~ND2. $P_p = 2$~~ ND1, where $\hat{P}_p$ denotes the wake model estimate for P_p. $\hat{P}_p = 2$ will lead to an underestimate of the power production loss due to yaw misalignment and ~~$P_p = 4$~~ $\hat{P}_p = 4$ will lead to an overestimate. Given that the value of P_p is turbine-specific, the influence of the P_p uncertainty described in this section should be considered relative to the true value of $P_p = 3$, and the conclusions apply with respect to the scaled values of $\hat{P}_p / P_p$. For a different turbine model with $P_p = 2$, for example, similar values of $\hat{P}_p / P_p$ would yield qualitatively similar results.

The power productions as a function of the yaw update steps for Cases ~~ND4 and ND5~~ NDP2 and NDP4 are shown in Figure 17. Case ~~ND4 with $P_p = 2$~~ NDP2 with $\hat{P}_p = 2$ has 3.0% less power production than baseline greedy operation while Case ~~ND5~~

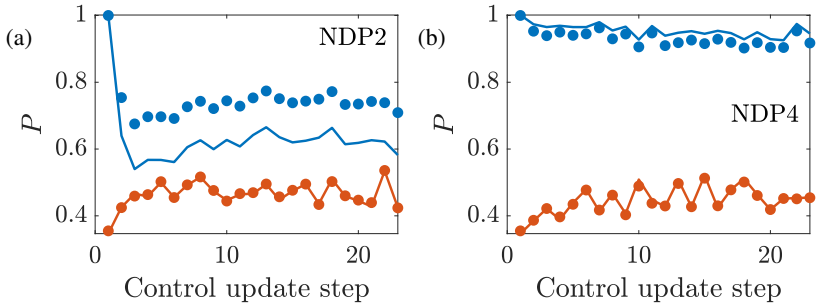

Figure 19. Time averaged power production for the first and second wind turbines in the wind farm as a function of the control update steps for online control using the initial parameters to initialize the next state and (a) ~~$P_p = 2$~~ $\hat{P}_p = 2$ (~~ND4~~NDP2) and (b) ~~$P_p = 4$~~ $\hat{P}_p = 4$ (~~ND5~~NDP4). The LES power production is given by P and the wake model state estimation is given by $\hat{P}$.

~~with $P_p = 4$~~ NDP4 with $\hat{P}_p = 4$ has 5.1% more power than baseline control. Case ~~ND2 and ND5 are significantly better than ND4. With $P_p = 2$~~ND1 and NDP4 have significantly higher power production than NDP2. With $\hat{P}_p = 2$, the model prediction for the optimal yaw misalignment angles are high, with the first three upwind turbines misaligning by almost $\gamma = 40°$ (Figure 18(a)). With ~~$P_p = 4$~~ $\hat{P}_p = 4$, the penalty for yaw misalignment is significant and no turbine misaligns more than $\gamma = 20°$ (Figure 18(b)). For the present conventionally neutral ABL and ADM implemented, $3 < P_p < 4$ for the leading upwind turbine. The success of Case ~~ND5 with $P_p = 4$~~ NDP4 with $\hat{P}_p = 4$ suggests that small yaw misalignments can still increase the wind farm power production significantly with respect to the baseline greedy control.

The LES power productions and EnKF state estimated powers as a function of the yaw control updates are shown for the two ~~P_p~~ $\hat{P}_p$ cases in Figure 19. For Case ND4, the upwind turbine power production is significantly over-predicted. The EnKF does not estimate the state for the most upwind turbine since there are no wake model parameters which influence its production. The power production for the second wind turbine is accurately estimated even with ~~$P_p = 2$~~ $\hat{P}_p = 2$. This again shows that the state estimation with a two-parameter model is likely overparameterized where the EnKF is ~~making up~~ compensating for the incorrect P_p model by altering k_w and σ_0 unphysically, although the consequence of this effect in the accuracy of the power predictions will be discussed in §4.4. The power productions and EnKF estimations for the first two wind turbines for Case ND5 show that ~~$P_p = 4$~~ $\hat{P}_p = 4$ is a more accurate estimate than ~~$P_p = 2$~~ $\hat{P}_p = 2$. Again, the downwind turbine power is estimated accurately with the incorrect value of ~~P_p~~ $\hat{P}_p$.

The comparison between the wake model power predictions against the LES power production are shown in Figure 20. With ~~$P_p = 2$~~ $\hat{P}_p = 2$ (Figure 20(a)), the wake model significantly overpredicts the power production of the wind turbine array with expected power increases over the baseline of 25% but a power decrease with respect to the baseline realized. On the other hand, with ~~$P_p = 4$~~ $\hat{P}_p = 4$ (Figure 20(b)), the wake model underpredicts the power production of the wind turbine array for nearly all control update steps. ~~Interestingly, Case ND5 outperforms Case ND2 ($P_p = 3$), but not significantly.~~ Comparing Figures 15(b) and 20(b), it is clear that, in this simulation, the lifting line model prediction of downwind turbine power is less conservative as a function of increasing γ. Therefore, the model is likely slightly over-estimating the true optimal yaw misalignment angle magnitudes when $P_p = 3$.

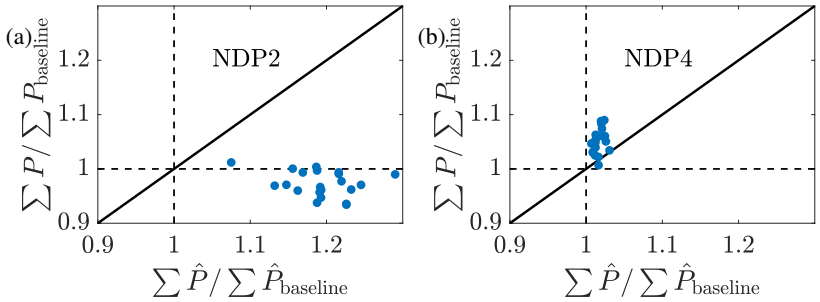

Figure 20. Relationship between the LES wind farm power production compared to the wake model wind farm power production prediction for online control using the initial parameters to initialize the next state and (a) ~~$P_p = 2$~~ $\hat{P}_p = 2$ (NDP2) and (b) ~~$P_p = 4$~~ $\hat{P}_p = 4$ (NDP4). The LES power production is given by P and the wake model prediction is given by $\hat{P}$.

Overall, the sensitivity analysis on P_p suggests that given a model application where P_p is unknown, a conservative estimation should be taken~~(e. g. $P_p = 4$).~~ . With the present data-driven dynamic controller, underestimating P_p leads to the wake model estimating a state which would lead to high wake losses with baseline greedy control. There is no pathway for the state estimation to discern the discrepancy between an incorrect P_p model or, for example, changing atmospheric conditions which are giving rise to worsening wake losses given baseline control. Future work should focus on methodologies to robustly estimate P_p from SCADA data. Further, the potential deviation of the wind turbine thrust from $\cos^2(\gamma)$ (Bastankhah and Porté-Agel, 2016) should be investigated in a similar manner as P_p in future work.

4.4 Accuracy of wake model predictions

The accuracy of the wake model power predictions are assessed in this section by comparing the LES power measurements to the wake model power predictions from the previous time step. As detailed in Section 3, the simulation is initialized with greedy yaw alignment which is held fixed for n_T time steps (control update 1), after which yaw misalignment angles are implemented for n_T steps (control update 2). The yaw angles are subsequently updated dynamically every n_T simulation steps. At control update 1, the previous n_T steps of yaw aligned operation are used to compute P_{baseline}, the time averaged power production for each wind turbine. P_{baseline} is used to estimate k_w and σ_0 using the EnKF such that $|P_{\text{baseline}} - \hat{P}_{\text{baseline}}|$ is minimized. With the estimated model parameters, the optimal yaw misalignment angles are computed for each wind turbine. Using k_w and σ_0 estimated and the optimal yaw angles computed at control update 1, $\hat{P}_{\text{yaw}}$ is predicted which is attempting to represent P_{yaw}, the average power production over the n_T steps following control update 1. The computation of P_{yaw} is completed at control update 2 and can be compared directly to $\hat{P}_{\text{yaw}}$ to validate the predictive capabilities of the lifting line model and the estimated model parameters. In short, $\hat{P}_{\text{baseline}}$ represented P_{baseline} and it is an estimation or fit because the model had knowledge of P_{baseline}. $\hat{P}_{\text{yaw}}$ is a prediction since the model had no knowledge of P_{yaw}. The LES measured and wake model estimated and predicted power productions are shown in Figure 21 for ~~$P_p = 2$~~ $\hat{P}_p = 2$, 3, and 4.

The mean absolute error for the lifting line model power estimation was 0.0037 for all three cases since P_p does not affect the fitting with yaw aligned control enforced. The mean absolute errors for the lifting line model power predictions were 0.044,

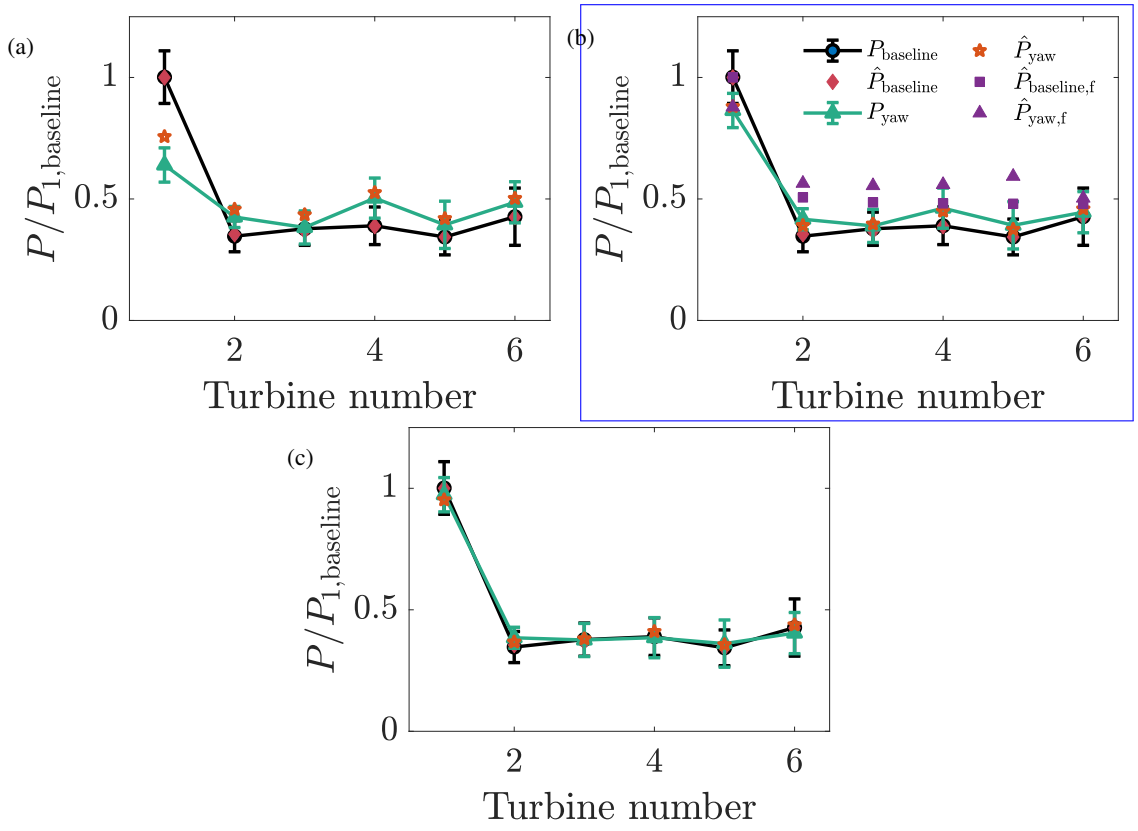

Figure 21. Wind turbine power production from LES P and wake model $\hat{P}$. $P_{1,\mathrm{baseline}}$ is the LES power production for the leading upwind turbine from control update step 1 where the wind farm is operated with greedy baseline control. $\hat{P}_{\mathrm{baseline}}$ is the wake model fit to P_{baseline} using EnKF estimation. P_{yaw} is the LES power production for control update step 2 with yaw misalignment incorporated. $\hat{P}_{\mathrm{yaw}}$ is the wake model prediction of P_{yaw} using k_w and σ_0 fit based on control update step 1 and with the optimal yaw misalignment angles which were implemented by control update step 1. The wake model estimate for P_p, given by $\hat{P}_p$ is (a) ~~$P_p = 2$~~$\hat{P}_p = 2$, (b) ~~$P_p = 3$~~$\hat{P}_p = 3$, and (c) ~~$P_p = 4$~~$\hat{P}_p = 4$. The error bars represent one standard deviation in the power data as a function of time. The subscript 'f' denotes power predictions from the FLORIS wake model (Annoni et al., 2018) with the Gaussian wake model (Bastankhah and Porté-Agel, 2014) and model parameters prescribed by Niayifar and Porté-Agel (2016).

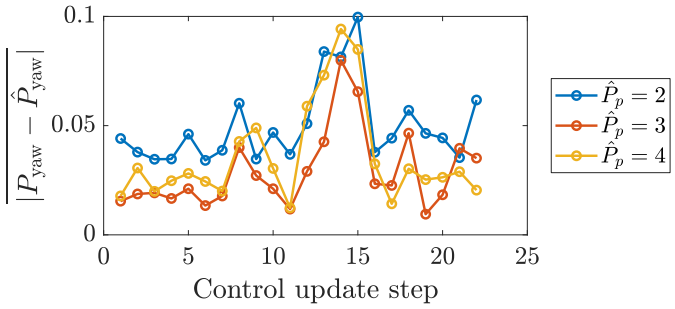

Figure 22. The mean absolute errors for the lifting line model predictions as a function of the control update step for the conventionally neutral ABL with ~~$P_p = 2$~~$\hat{P}_p = 2$, 3, and 4.

0.015, and 0.018, given as a fraction of $P_{1,\text{baseline}}$, for ~~$P_p = 2$~~$\hat{P}_p = 2$, 3, and 4, respectively. The mean absolute errors as a function of the control update steps for the three simulations are shown in Figure 22. The average over the control update steps of the mean absolute errors for the three cases are 0.05, 0.029, and 0.036 for ~~$P_p = 2$~~$\hat{P}_p = 2$, 3, and 4, respectively. Qualitatively, ~~$P_p = 3$~~ $\hat{P}_p = 3$ and 4 results in predictions which are accurate and within one standard deviation of the mean. ~~$P_p = 2$~~ $\hat{P}_p = 2$ results in more inaccurate predictions, with elevated inaccuracy for the leading upwind turbine. Overall, these results, in tandem with the field experiment results of Howland et al. (2019), suggest that the lifting line model (Shapiro et al., 2018) provides accurate predictions of the power production of wind farms within yaw misalignment given data-driven calibration to yaw aligned operational data.

The baseline and yaw misaligned power predictions using the FLORIS wake model package (Annoni et al., 2018) is also shown in Figure 21. The FLORIS model implementation uses the Gaussian wake model (Bastankhah and Porté-Agel, 2014) with the wake spreading rate k^* approximated using the empirical LES fit between k^* and the turbulence intensity given by Niayifar and Porté-Agel (2016). Since the Gaussian wake model parameters are not calibrated to the site-specific LES of this wind farm, the inaccuracy in representing P_{baseline} is expected according to the typical fidelity of engineering wake models (Stevens and Meneveau, 2017). The mean absolute error for the power production prediction in yaw misalignment averaged over the six wind turbines in the array is $0.02P_{1,\text{baseline}}$ and $0.11P_{1,\text{baseline}}$ for the lifting line model with data assimilation and the Gaussian model with an empirical wake spreading rate as a function of turbulence intensity, respectively. $P_{1,\text{baseline}}$ is the power production of the leading upwind turbine in greedy control. The EnKF data assimilation has reduced the error in the prediction of the power production in yaw misalignment by an order of magnitude compared to *a priori* prescribed empirical model parameters. Since the greedy wake losses in FLORIS differ from the LES power production, FLORIS will also predict different yaw misalignment angles in its model-based optimization. For greenfield applications before wind farm construction, SCADA data is not available and data assimilation methods cannot be used, necessitating empirical methods such as those suggested by Niayifar and Porté-Agel (2016). For operational wind farm control optimization, site-specific data assimilation increases the accuracy of the model predictions (Figure 21(b)).

4.5 Influence of the wind farm alignment

The wake losses and potential for wake steering to increase wind turbine array power production depends on the wind turbine layout (see e.g. experiments by Bossuyt et al., 2017). In the previous section, the six wind turbines were aligned at an angle of 18° from the horizontal (Figure 3). The mean wind direction at hub height is approximately 15°-16° in this conventionally neutral ABL. In this section, the wind turbine column alignment is changed to 14° from the horizontal and the array is embedded within the same conventionally neutral ABL. As a result of this array alignment, the optimal yaw misalignment angles will change from positive (counter-clockwise rotation viewed from above) to negative (clockwise). It should be noted that this sensitivity analysis is not a controlled experiment to test the benefit of yawing in opposite directions since asymmetries exist in the conventionally neutral ABL as a result of the veer angle and the magnitude of partial waking is not held fixed between the two layouts.

Yaw misalignment angles for each turbine in the wind farm for online control using (a) the initial parameters to initialize the next state (ND141) and (b) static state estimation parameters (ND142) for wind farm alignment at 14°.

Time averaged wind farm power production as a function of the control update step for online control using (a) the initial parameters to initialize the next state (ND141) and (b) static state estimation parameters for wind farm alignment at 14° (ND142). The wind farm power is normalized by the power production of the aligned wind farm case.

For the wind turbine array aligned at 14°, the dynamic wake steering controller is tested with dynamic (ND141) and static state estimation (ND142). With a wind farm alignment along 14° and the mean wind direction at hub height of approximately 15°-16°, the optimal yaw misalignment angles are negative (clockwise viewed from above). The yaw misalignment angles implemented as a function of the control update steps are shown in Figure E1 for dynamic and static state estimation architectures. The qualitative magnitude of the yaw misalignment angles are similar to the angles selected for the 18° alignment case (Section 4.1).

The power productions for the two wake steering controllers are shown in Figure E2. The temporally averaged power production increase over baseline, greedy operation is 1.1% and 1.0% for the dynamic and static state estimation cases, respectively. There is no significant difference in the mean power production between these two state estimation methodologies for this wind farm alignment (see Table 1). Further, neither wake steering control case increases power significantly over greedy control. While the power production increase over the greedy control is less for the 14° case with negative yaw misalignment than for the 18° case with positive yaw misalignment this is not a controlled experiment since the degree of partial waking is different between the two cases. The wind farm has more direct wake interactions, with less partial waking, for the 14° alignment as evidenced by the lower power production in greedy control (Table 1). Previous simulations have shown that for a controlled experiment of direct wind farm alignment, positive yaw misalignment (counter-clockwise) is superior to negative yaw misalignment (clockwise) (see e.g. Fleming et al., 2015; Miao et al., 2016), although this will depend on the specific ABL and wind farm layout simulated. Archer and Vasel-Be-Hagh (2019) proposed that this difference is a function of Coriolis forces in the ABL, although future work should quantify the effect of latitude and hemisphere locations as well as the influence of non-traditional effects (Howland et al., 2020b). The degree of power production increase as a result of wake steering is a strong

~~function of the wind farm alignment with respect to the wind direction at hub height, the turbine spacing, the shear, and veer. The present simulations reveal that it is reasonable to capture increases in power production with negative (clockwise) wake steering even with a wind turbine model with $P_p \approx 3$.~~

5 Conclusions

A suite of large eddy simulations has been performed to characterize the performance of a dynamic, closed-loop wake steering wind farm control strategy. The controller was designed for the application of real-time utility-scale wind farm control based on only SCADA data without requiring a LiDAR on site. ~~The physics- and data-driven ensemble Kalman filter and wake model based controller was validated in uniform inflow LES before being tested in conventionally neutral ABL conditions with Coriolis, shear, and veer. The~~ The analytic gradient ascent optimal yaw selection allows for real-time dynamic wind farm control. The ~~sensitivity of the power production increase via wake steering over greedy, yaw aligned control was characterized as a function of the controller architecture, P_p, state estimation architecture, wind farm layout, and ABL conditions.~~ main technical contribution of this paper is the development of a closed-loop wake steering methodology for application in transient ABL flows which does not rely on an open-loop offline yaw misalignment lookup table calculation.

Within the statistically quasi-stationary conventionally neutral ABL, the optimal yaw misalignment angles do not change significantly with time. Within this simplified ABL environment, ~~a static wake steering strategy, where the yaw misalignments do not change, increased power production by 5.4% with respect to baseline greedy control. Dynamic wake steering with dynamic state estimation increased power production by 4.6%, slightly less than the static yaw misalignment strategy but not significantly~~wake steering control with fixed, lookup table yaw misalignment values, dynamic yaw values with continuous state estimation, and dynamic yaw values with fixed state estimation all yielded significantly more power than baseline control, although the differences between the three control architectures were not significant. The highest power production occurred with a wake steering strategy where the model parameters were fixed and the state estimation was not performed every control update step but the yaw misalignment angles were updated according to the local wind conditions. This result ~~indicates~~ suggests that in a lookup table wake steering approach, the wake model parameters should be tabulated and the yaw angles should be calculated on-the-fly given exact local wind conditions, rather than direct optimal yaw misalignment angle tabulation. ~~All three of these wake steering cases increased power significantly over greedy, aligned control although the differences between the three control architectures were not significant.~~

The importance of the model for individual wind turbine power production degradation as a function of the yaw misalignment angle, and in particular P_p, was demonstrated where ~~$P_p = 3$~~ $\hat{P}_p = 3$ or 4 lead to an increase in power production with respect to greedy operation while ~~$P_p = 2$~~ $\hat{P}_p = 2$ lead to a loss in power. ~~Wake steering cases with~~ , with the true $P_p = 3$ ~~and 4 led to a significant increase in power production compared to greedy control while $P_p = 2$ did not.~~ . Since P_p depends on the wind turbine model and ABL characteristics ~~and there is no accepted general framework for determining P_p~~, this should be investigated in future work. ~~With $P_p = 3$, the~~

The wake model does not capture all relevant physical phenomena present in this flow (see specific assumptions in wake model derivation in §2.1), but the power production is fit accurately as a function of time with the two parameter model. While this success may suggest that the site- and time-specific state estimation may correct for physics which are unresolved in the model, with $\hat{P}_p = P_p = 3$, the wake model makes accurate forecasts of the power production over a future time horizon given the yaw misalignment strategy that is implemented, provided that the wake model parameter modifications are constrained by the state estimation algorithm initialization as in Case ND1, rather than unconstrained as a function of time as in Case ND2. This accuracy gives confidence to the data-driven EnKF state estimation and lifting line wake model for the application of wake steering control. The combined lifting line model and EnKF state estimation has an order of magnitude reduced predictive error than the Gaussian wake model with an empirical wake spreading rate in this conventionally neutral ABL simulation.

~~The results are qualitatively similar when a wind farm of different alignment is embedded within the conventionally neutral ABL. The power production is decreased with a wind farm alignment of 14° compared to 18° and with a clockwise yaw misalignment compared to a counter-clockwise, although this was not a controlled experiment of the influence of the direction of yaw misalignment.~~ The magnitude of model parameter modifications as a function of time are implicitly constrained in this study by the hyperparameters of the EnKF estimation algorithm. Future work should investigate the predictive capabilities for combined data-driven and wake model approaches with explicit constraints on the model parameters.

While the conventionally neutral ABL cases were not designed to model a specific wind farm and to compare to field data, this LES testbed paradigm is useful for the rapid prototyping of optimal wind farm control architectures. The main purpose of this study was predominantly to establish the dynamic wake steering framework and perform sensitivity analysis on the controller architecture rather than the ABL or LES setup. The uncertainties and sensitivities in this study associated with the wall model, subfilter scale model, wind turbine model, and ABL characteristics such as boundary layer inversion height were not investigated in detail and are left for future work. More reliable and generalizable estimates for P_p ~~(?)~~(Liew et al., 2020) , or generally C_p as a function of γ, should be investigated. Future work should also investigate the influence of latitude and geostrophic wind direction on wake steering control performance (Howland et al., 2020b). Finally, the controller should be tested using other LES codes and in field experiments to assess the generalization of the results. Part 2 of this study will implement the dynamic optimal controller in transient ABL conditions such as the stable ABL and the diurnal cycle.

Code and data availability. The code is open-source and available at https://github.com/FPAL-Stanford-University/PadeOps. The GitHub repository branch for incompressible wind farm simulations is 'igridSGS.' The data will be open-access and published on the Stanford Digital Repository (https://sdr.stanford.edu/) upon publication.

Appendix A: EnKF test model problem

The state estimation EnKF algorithm and implementation is tested using a six wind turbine model wind farm with artificial data. Six 1.8 MW Vestas V80 wind turbines are modeled with incoming wind speed of $u_\infty = 7.5$ m/s. The turbines are

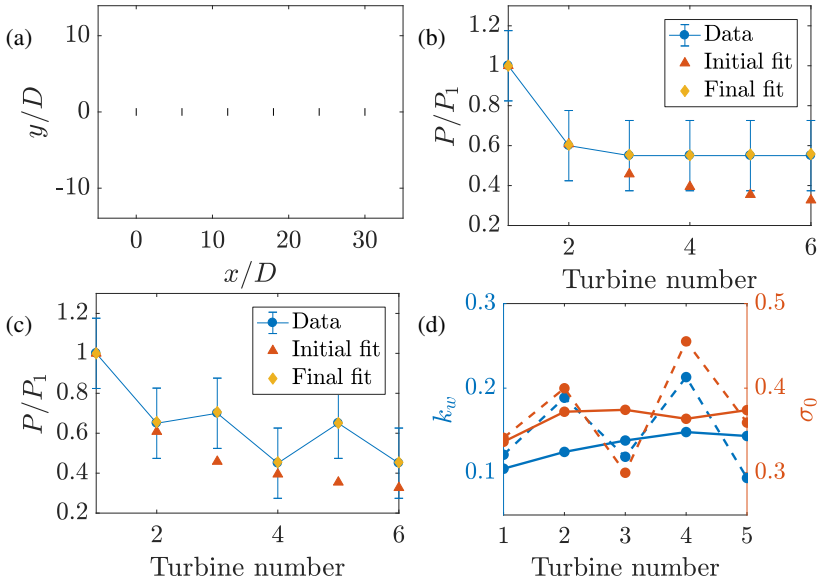

Figure A1. (a) Model problem setup. (b,c) The EnKF model fits for the model problem with two prescribed, artificial mean power profiles and Gaussian random noise. (d) Model parameters shown with solid (b) and dashed (c) lines. The wake model parameters for the last turbine downwind are not shown since they do not impact the state estimation accuracy.

spaced $6D$ apart in the streamwise direction and are directly aligned in the spanwise direction as shown in Figure A1(a). The test problem was used for hyperparameter selection to achieve estimations of the artificial power production with low mean absolute error. The parameters selected for the EnKF algorithm are $\sigma_{k_w} = 0.001$, $\sigma_{\sigma_0} = 0.001$, and $\sigma_P = 0.1$. The initial wake model parameters were selected as $k_w = 0.1$ and $\sigma_0 = 0.35$ for each wind turbine in the array. The model is run with a specified, artificial mean power production profile with Gaussian random noise superposed. The model is run over 1000 model time step iterations with $N_e = 100$. The initial and final model calibrations are shown in Figure A1(b,c). The EnKF combined with the lifting line model is able to fit the artificial wind farm data with sufficient accuracy for two different power production profiles.

As shown in Figure A1(b,c), the EnKF state estimation combined with the lifting line model are able to reproduce the power production for the artificial data to high accuracy. ~~The~~ While the ability for a ~~one or~~ two parameter analytic wake model to capture arbitrarily generated power production profiles should be investigated in future studies~~as the model may enforce unrealistic model parameters to represent neglected physics (Schreiber et al., 2019). The validity of~~ , this data-driven framework is validated in the LES test cases in a comparison between model power predictions and LES power measurements (Section ~~4)~~ 4.4) where the state estimation significantly reduces the power predictions compared to standard empirical wake model approaches.

Appendix B: ~~Extended conventionally neutral simulation~~

~~The conventionally neutral ABL Case ND2 is run for 50 control update steps and the results are shown in Figure D1. The controller does not become unstable as a function of time and the magnitude of yaw misalignment angles are approximately constant.~~

~~Wind farm (a) yaw misalignment angles, (b) k_w, and (c) σ_0 as a function of the control update steps for the extended ND2 case.~~

Appendix B: Influence of local atmospheric conditions on wind turbine array power production

The quantification of the influence of new control methods on the wind farm power production is challenging in an experimental setting. In a computational environment, simulations with identical initial conditions and fixed time stepping schemes can be used to quantify the influence of the operational modifications in a controlled experiment. In a field experiment environment, since wind conditions are constantly changing and are not repeatable due to the nature of atmospheric flows, this quantification is more challenging. Complex terrain and differences in the manufacturing and operation of turbines in standard control leads to substantial discrepancies in the instantaneous power production of freestream turbines at wind farms. Therefore, comparing yaw misaligned columns of turbines to yaw aligned leads to uncertainty in analysis. Further, conditional averages based on wind speed, direction, turbulence intensity, and atmospheric conditions may not sufficiently capture the potential physical mechanisms which influence power production. To quantify this impact in the present simulations, the power productions as a function of the control update steps can be compared to the first control update step in the statistically quasi-stationary conventionally neutral ABL flow. Inertial oscillations, turbulence, and sampling error will cause discrepancies between the first and subsequent control update steps even with the yaw aligned control strategy held fixed in the statistically quasi-stationary flow. The average power production compared to the first yaw control update step is 4.3% and 9.0% higher for the yaw aligned (Case NA) and dynamic closed-loop control (Case ~~ND2~~ND1), respectively. The increase observed in Case NA indicates that the simulation had not completely converged to the statistically quasi-stationary state upon control initialization although this does not affect the qualitative conclusions of Section 4. The true increase in power production due to wake steering in Case ~~ND2~~ ND1 compared to Case NA is 4.6% over the same simulation temporal window. These results highlight the need to develop robust statistical methods to analyze the impact of changing wind farm control strategies compared to the baseline.

Appendix C: Approximate advection timescale

Upon the yaw misalignment of an upwind turbine, there is a time lag associated with the advection time scale of the flow for the control decision to influence a downwind turbine. While the advection time depends on the length scale of the turbulent eddy (Del Álamo and Jiménez, 2009; Yang and Howland, 2018; Howland and Yang, 2018), the mean flow advection approximately follows the mean wind speed in wind farms (Taylor, 1938; Lukassen et al., 2018). The number of simulation

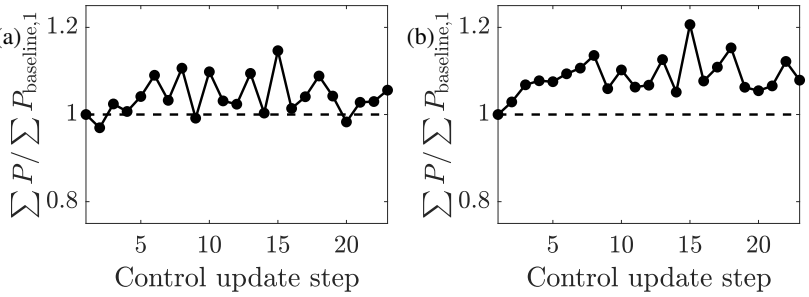

Figure B1. Time averaged power production as a function of time normalized by the time averaged power production of the first control update step for yaw aligned greedy control. (a) Yaw aligned greedy control (Case NA) and (b) closed-loop dynamic control (Case ~~ND2~~ND1).

time steps associated with the approximate advection time between the first and last turbines is computed as

$$T = \frac{\Delta s_x}{\overline{u}_{\text{hub}} \Delta t}, \tag{C1}$$

where Δs_x is the distance between the first and last turbine in the streamwise direction and $\overline{u}_{\text{hub}}$ is the mean streamwise velocity at the wind turbine model hub height at the leading turbine in the farm. The simulation time step is fixed and is Δt, which corresponds to a CFL of less than 1 persistently during runtime. In the computation of wind farm statistics for the utilization of static wake models, the advection time scale is accounted for by initializing the time averaging two advection time scales $T_a = 2T$ after the yaw misalignments for the wind turbine array have been updated. To account for errors associated with the simple advection model, the time lag is taken as double the advection time scale, $T_a = 2T$, although this advection time scale did not have a statistically significant influence on the results as shown in Table 1and Figure 5.

Appendix D: Extended conventionally neutral simulation

The conventionally neutral ABL Case ND1 is run for 50 control update steps and the results are shown in Figure D1. The controller does not become unstable as a function of time and the magnitude of yaw misalignment angles are approximately constant.

Appendix E: Influence of the wind farm alignment in the conventionally neutral ABL

The wake losses and potential for wake steering to increase wind turbine array power production depends on the wind turbine layout (see e.g. experiments by Bossuyt et al., 2017). In the previous section, the six wind turbines were aligned at an angle of 18° from the horizontal (Figure 3). The mean wind direction at hub height is approximately 15°-16° in this conventionally neutral ABL. In this section, the wind turbine column alignment is changed to 14° from the horizontal and the array is embedded within the same conventionally neutral ABL. As a result of this array alignment, the optimal yaw misalignment angles will change from positive (counter-clockwise rotation viewed from above) to negative (clockwise). It should be noted

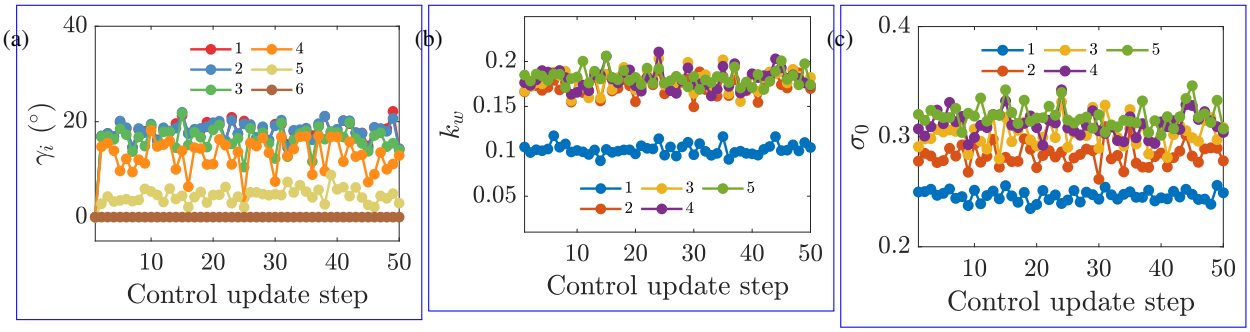

Figure D1. Wind farm (a) yaw misalignment angles, (b) k_w, and (c) σ_0 as a function of the control update steps for the extended ND1 case.

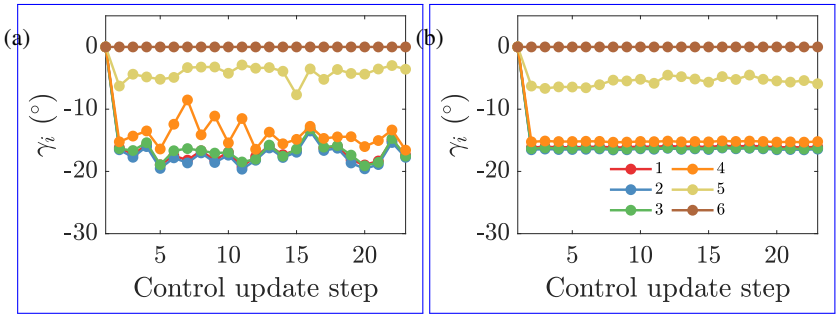

Figure E1. Yaw misalignment angles for each turbine in the wind farm for online control using (a) the initial parameters to initialize the next state (ND141) and (b) static state estimation parameters (ND142) for wind farm alignment at 14°.

that this sensitivity analysis is not a controlled experiment to test the benefit of yawing in opposite directions since asymmetries exist in the conventionally neutral ABL as a result of the veer angle and the magnitude of partial waking is not held fixed between the two layouts.

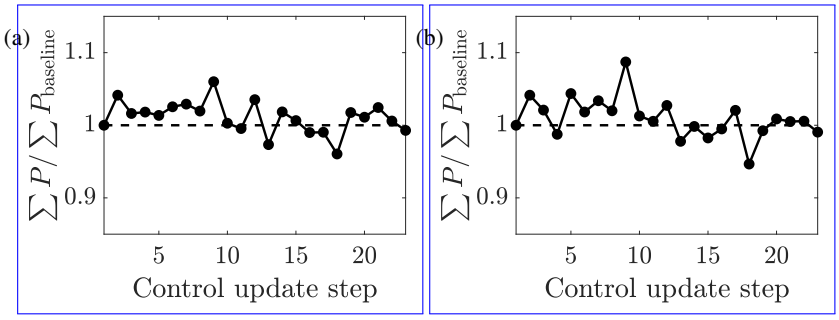

Figure E2. Time averaged wind farm power production as a function of the control update step for online control using (a) the initial parameters to initialize the next state (ND141) and (b) static state estimation parameters for wind farm alignment at 14° (ND142). The wind farm power is normalized by the power production of the aligned wind farm case.

For the wind turbine array aligned at 14°, the dynamic wake steering controller is tested with dynamic (ND141) and static state estimation (ND142). With a wind farm alignment along 14° and the mean wind direction at hub height of approximately 15°-16°, the optimal yaw misalignment angles are negative (clockwise viewed from above). The yaw misalignment angles implemented as a function of the control update steps are shown in Figure E1 for dynamic and static state estimation architectures. The qualitative magnitude of the yaw misalignment angles are similar to the angles selected for the 18° alignment case (Section 4.1).

The power productions for the two wake steering controllers are shown in Figure E2. The temporally averaged power production increase over baseline, greedy operation is 1.1% and 1.0% for the dynamic and static state estimation cases, respectively. There is no significant difference in the mean power production between these two state estimation methodologies for this wind farm alignment (see Table 1). Further, neither wake steering control case increases power significantly over greedy control. While the power production increase over the greedy control is less for the 14° case with negative yaw misalignment than for the 18° case with positive yaw misalignment this is not a controlled experiment since the degree of partial waking is different between the two cases. The wind farm has more direct wake interactions, with less partial waking, for the 14° alignment as evidenced by the lower power production in greedy control (Table 1). Previous simulations have shown that for a controlled experiment of direct wind farm alignment, positive yaw misalignment (counter-clockwise) is superior to negative yaw misalignment (clockwise) (see e.g. Fleming et al., 2015; Miao et al., 2016), although this will depend on the specific ABL and wind farm layout simulated. Archer and Vasel-Be-Hagh (2019) proposed that this difference is a function of Coriolis forces in the ABL, although future work should quantify the effect of latitude and hemisphere locations as well as the influence of non-traditional effects (Howland et al., 2020b). The degree of power production increase as a result of wake steering is a strong function of the wind farm alignment with respect to the wind direction at hub height, the turbine spacing, the shear, and veer. The present simulations reveal that it is reasonable to capture increases in power production with negative (clockwise) wake steering even with a wind turbine model with $P_x \approx 3$.

Appendix F: Dynamic wake steering uniform inflow LES

In this section, the dynamic closed-loop wake steering controller described by Figure 1 will be used in LES of two turbines operating in uniform inflow. Uniform inflow is not physical, and depending on the LES resolution, the results will be dependent on the sub-grid scale model due to the sharp shear layer and reduced mixing of the test case (see detailed discussion by Howland et al., 2016). However, uniform inflow provides a useful statistically stationary test case for the validation of the closed-loop wake steering methodology. The domain has lengths of $25D$, $10D$, and $10D$ in the x, y, and z directions, respectively, and the number of grid points are 128, 64, and 64. Two actuator disk model wind turbines are simulated in uniform inflow with slip walls on all sides and a fringe region at the domain exit to force the inflow to a uniform profile. The fringe is used in the last 25% of the computational x domain. The turbines are located $4D$ apart in the streamwise direction and are misaligned by $0.25D$ in the spanwise direction as shown in Figure F1. Due to the spanwise misalignment, the preferential yaw misalignment direction for the upwind turbine is positive (counter-clockwise rotation viewed from above).

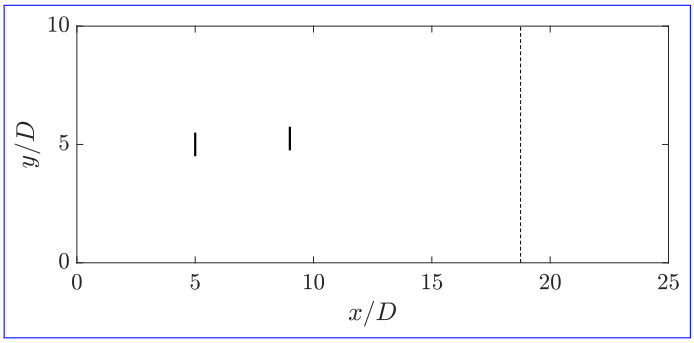

Figure F1. Uniform inflow LES simulation actuator disk model layout. The fringe region is represented by the dashed black line and the wind turbines are shown as solid black lines.

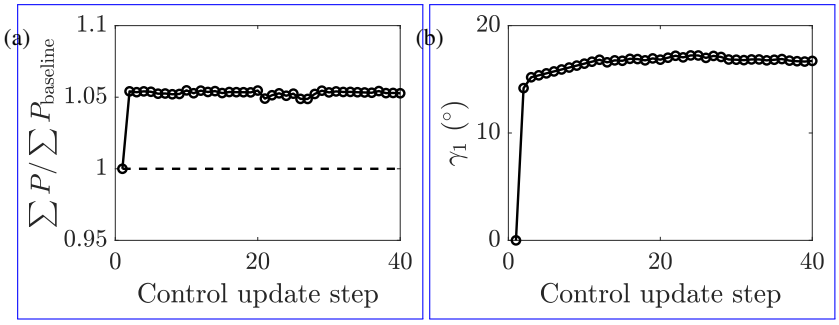

Figure F2. Two wind turbine model uniform inflow LES (a) power production. (b) The yaw misalignment angle γ for the upwind turbine. The downwind turbine remains yaw aligned during the simulation.

The flow is statistically stationary after the initial startup transient has decayed and therefore the optimal yaw misalignment angles for the two wind turbines are not a function of time. The flow is initialized with $u = 1$. Upon statistical stationarity, the closed-loop wake steering controller is initialized and the flow is run for $n_T = 10000$ LES time steps to ensure sufficient averaging. The time averaging is initialized following the advection time of the wind farm (see Section C) and therefore there are $n_T - T_a$ timesteps within each time averaging window.

The sum of power production for the two turbine pair as a function of the control update steps is shown in Figure F2(a). The power production is normalized by the greedy control simulation. The power production for the first yaw controller update time step is equal to 1 since yaw misalignment has not been implemented and the model is gathering power production data to be used for the first EnKF data assimilation pass. The power production increases in the second time step when yaw misalignment in incorporated for the upwind turbine (Figure F2(b)). The controller correctly commands the upwind turbine to positive yaw misalignment. While the flow is statistically stationary, the upwind turbine yaw misalignment angle changes marginally after the second time step. These changes can be attributed to modifications to the wake model parameters as a function of time as estimated by the EnKF (Figure F3(a)). The estimated model parameters vary in time in this statistically stationary flow due

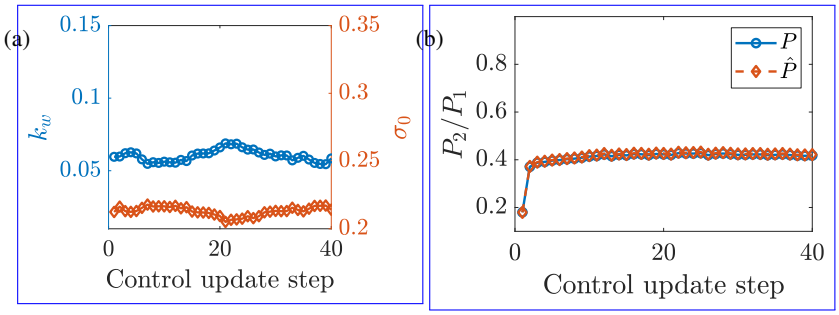

Figure F3. Two wind turbine model uniform inflow LES (a) k_w and σ_0 for the upwind turbine and (b) $\hat{P}$ and P for the downwind turbine.

to standard error of the mean with limited samples within a given time window of length T, due to the influence of the yaw misalignment of the dynamics on the wake, and due to the limited number of ensembles N_e in the EnKF.

The wake model parameters have a functional dependence on the yaw misalignment of the turbines within the wind farm. The wake of a yaw misaligned turbine is narrower than the same turbine when yaw aligned (Archer and Vasel-Be-Hagh, 2019). The wake spreading rate k_w dictates the wake recovery rate. Yaw misalignment also reduces the axial induction factor of the wind turbine and therefore affects the wake recovery. Further, since wind turbines in yaw misalignment generate large-scale counter rotating vortices (Howland et al., 2016), the wake recovery rate will likely be enhanced in yaw misalignment (Fleming et al., 2018) due to a reduction in the axial induction and yaw added recovery (King et al., 2020). As a result of these vortices, the wake will have top-down asymmetry and this will influence σ_0. While the present model neglects the vertical dimension, the development of a controls-oriented model which incorporates the curled wake asymmetry is ongoing (Martínez-Tossas et al., 2019). Future work should characterize the influence of yaw misalignment on the wake spreading rate.

The state-estimated power production for the downwind turbine is compared to the LES power production in Figure F3(b). The downwind turbine's power production in the greedy control strategy is low (approximately $0.2P_1$) due to the freestream inflow condition and close streamwise direction spacing. The EnKF results in an accurate power production estimation using the lifting line model. While the wake model parameters are changing as a function of time (Figure F3(a)), the power production estimate for the downwind turbine is not significantly affected. The wake model parameters k_w and σ_0 are anti-correlated as a function of time. Within the two-parameter lifting line model, increasing k_w or σ_0 reduces the wake effect for the downwind turbine. With the LES power production of the downwind turbine and the yaw misalignment of the upwind turbine approximately fixed, the state estimation increases one parameter and reduces the other parameter to remain consistent in the estimation of the downwind power. This indicates, similarly to the results in Appendix A, that the two parameter lifting line model may be overparameterized, and a single parameter model, with fixed σ_0 for example, may suffice (Shapiro et al., 2019). The accuracy of the EnKF state estimation and lifting line model in the prediction of the power production in yaw misalignment is tested in Section 4.4. This accuracy will implicitly measure the impact of the site-specific fitting in the model.

The control architecture used in the uniform inflow case is the same as Case ND2, where the estimated model parameters from the previous time step are used to initialize the parameters for the estimation at the next time step. As discussed in

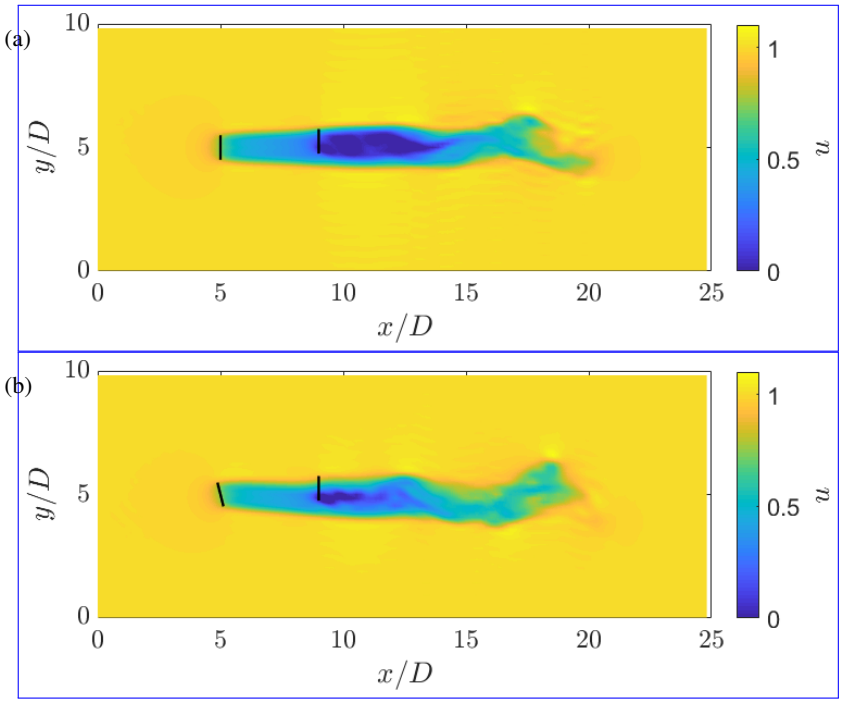

Figure F4. Two wind turbine model uniform inflow LES instantaneous streamwise velocity u snapshot with (a) no yaw misalignment (b) after the last time step of dynamic wake steering.

§4.2, this allows the parameters to change significantly over time compared to their initialization state. By fixing the EnKF initialization (as done in Case ND1), the modifications to the wake model parameters are limited by the hyperparameters σ_{k_w} and σ_{σ_0}. Since there is no wake impinging on the upwind turbine, the state estimation has no impact on the power prediction of the upwind turbine since there are no wake model parameters to estimate. The accuracy of the upwind turbine model prediction will be governed by the fidelity of the cosine model and P_p, given by Eq. 6.

The instantaneous streamwise velocity is visualized in Figures F4(a) and (b) for the baseline greedy yaw control and the optimal yaw misalignment angle, respectively. As a result of the yaw misalignment, the wake is partially laterally deflected away from the downwind turbine. The yaw misalignment increases the magnitude of the streamwise velocity in the wake region.

Author contributions. M.F.H., S.K.L., and J.O.D. conceived the work. A.S.G. and M.F.H. developed the LES code. M.F.H. conducted analysis. M.F.H. wrote the manuscript. All authors contributed to edits.

Competing interests. The authors declare no conflicts of interest.

Acknowledgements. M.F.H. is funded through a National Science Foundation Graduate Research Fellowship under Grant No. DGE-1656518 and a Stanford Graduate Fellowship. A.S.G. was funded by Tomkat Center for Sustainable Energy at Stanford University. S.K.L. acknowledges partial support from NSF-CBET-1803378. All simulations were performed on Stampede2 supercomputer under the XSEDE project ATM170028. The authors would also like to thank the anonymous referees for their thoughtful comments and contribution to this work.

References

Adaramola, M. and Krogstad, P.-Å.: Experimental investigation of wake effects on wind turbine performance, Renewable Energy, 36, 2078–2086, 2011.

Allaerts, D. and Meyers, J.: Large eddy simulation of a large wind-turbine array in a conventionally neutral atmospheric boundary layer, Physics of Fluids, 27, 065 108, 2015.

Annoni, J., Gebraad, P. M., Scholbrock, A. K., Fleming, P. A., and Wingerden, J.-W. v.: Analysis of axial-induction-based wind plant control using an engineering and a high-order wind plant model, Wind Energy, 19, 1135–1150, 2016.

Annoni, J., Fleming, P., Scholbrock, A., Roadman, J., Dana, S., Adcock, C., Porte-Agel, F., Raach, S., Haizmann, F., and Schlipf, D.: Analysis of control-oriented wake modeling tools using lidar field results, Wind Energy Science, 3, 819–831, 2018.

Archer, C. L. and Vasel-Be-Hagh, A.: Wake steering via yaw control in multi-turbine wind farms: Recommendations based on large-eddy simulation, Sustainable Energy Technologies and Assessments, 33, 34–43, 2019.

Barthelmie, R. J., Hansen, K., Frandsen, S. T., Rathmann, O., Schepers, J., Schlez, W., Phillips, J., Rados, K., Zervos, A., and Politis, E.: Modelling and measuring flow and wind turbine wakes in large wind farms offshore, Wind Energy, 12, 431–444, 2009.

Bastankhah, M. and Porté-Agel, F.: A new analytical model for wind-turbine wakes, Renewable Energy, 70, 116–123, 2014.

Bastankhah, M. and Porté-Agel, F.: Experimental and theoretical study of wind turbine wakes in yawed conditions, Journal of Fluid Mechanics, 806, 506–541, 2016.

Bastankhah, M. and Porté-Agel, F.: Wind tunnel study of the wind turbine interaction with a boundary-layer flow: Upwind region, turbine performance, and wake region, Physics of Fluids, 29, 065 105, 2017.

Bastankhah, M. and Porté-Agel, F.: Wind farm power optimization via yaw angle control: A wind tunnel study, Journal of Renewable and Sustainable Energy, 11, 023 301, 2019.

Basu, S., Holtslag, A. A., Van De Wiel, B. J., Moene, A. F., and Steeneveld, G.-J.: An inconvenient "truth" about using sensible heat flux as a surface boundary condition in models under stably stratified regimes, Acta Geophysica, 56, 88–99, 2008.

Bauweraerts, P. and Meyers, J.: On the Feasibility of Using Large-Eddy Simulations for Real-Time Turbulent-Flow Forecasting in the Atmospheric Boundary Layer, Boundary-Layer Meteorology, 171, 213–235, 2019.

Bilgili, M., Ozbek, A., Sahin, B., and Kahraman, A.: An overview of renewable electric power capacity and progress in new technologies in the world, Renewable and Sustainable Energy Reviews, 49, 323–334, 2015.

Bitar, E. Y., Rajagopal, R., Khargonekar, P. P., Poolla, K., and Varaiya, P.: Bringing wind energy to market, IEEE Transactions on Power Systems, 27, 1225–1235, 2012.

Boersma, S., Gebraad, P., Vali, M., Doekemeijer, B., and Van Wingerden, J.: A control-oriented dynamic wind farm flow model:"WFSim", in: Journal of Physics: Conference Series, vol. 753, p. 032005, IOP Publishing, 2016.

Boersma, S., Doekemeijer, B., Gebraad, P. M., Fleming, P. A., Annoni, J., Scholbrock, A. K., Frederik, J., and van Wingerden, J.-W.: A tutorial on control-oriented modeling and control of wind farms, in: 2017 American Control Conference (ACC), IEEE, 2017.

Boersma, S., Doekemeijer, B., Vali, M., Meyers, J., and van Wingerden, J.-W.: A control-oriented dynamic wind farm model: WFSim, Wind Energy Science, 3, 75–95, 2018.

Borenstein, S.: The private and public economics of renewable electricity generation, Journal of Economic Perspectives, 26, 67–92, 2012.

Bossuyt, J., Howland, M. F., Meneveau, C., and Meyers, J.: Measurement of unsteady loading and power output variability in a micro wind farm model in a wind tunnel, Experiments in Fluids, 58, 1, 2017.

Burton, T., Jenkins, N., Sharpe, D., and Bossanyi, E.: Wind Energy Handbook, John Wiley & Sons, 2011.

Calaf, M., Meneveau, C., and Meyers, J.: Large eddy simulation study of fully developed wind-turbine array boundary layers, Physics of fluids, 22, 015 110, 2010.

Campagnolo, F., Petrović, V., Bottasso, C. L., and Croce, A.: Wind tunnel testing of wake control strategies, in: 2016 American Control Conference (ACC), pp. 513–518, IEEE, 2016a.

Campagnolo, F., Petrović, V., Schreiber, J., Nanos, E. M., Croce, A., and Bottasso, C. L.: Wind tunnel testing of a closed-loop wake deflection controller for wind farm power maximization, in: Journal of Physics: Conference Series, vol. 753, p. 032006, IOP Publishing, 2016b.

Ciri, U., Rotea, M. A., and Leonardi, S.: Model-free control of wind farms: A comparative study between individual and coordinated extremum seeking, Renewable energy, 113, 1033–1045, 2017.

Cleary, E., Garbuno-Inigo, A., Lan, S., Schneider, T., and Stuart, A. M.: Calibrate, Emulate, Sample, arXiv preprint arXiv:2001.03689, 2020.

Del Álamo, J. C. and Jiménez, J.: Estimation of turbulent convection velocities and corrections to Taylor's approximation, Journal of Fluid Mechanics, 640, 5–26, 2009.

Doekemeijer, B., Boersma, S., Pao, L. Y., and van Wingerden, J.-W.: Ensemble Kalman filtering for wind field estimation in wind farms, in: 2017 American Control Conference (ACC), pp. 19–24, IEEE, 2017.

Doekemeijer, B. M., Boersma, S., Pao, L. Y., Knudsen, T., and van Wingerden, J.-W.: Online model calibration for a simplified LES model in pursuit of real-time closed-loop wind farm control, Wind Energy Science Discussions, 2018, 1–30, 2018.

EIA: Annual Energy Outlook (AEO2018), 2018.

Evensen, G.: The ensemble Kalman filter: Theoretical formulation and practical implementation, Ocean dynamics, 53, 343–367, 2003.

Fleming, P., Scholbrock, A., Jehu, A., Davoust, S., Osler, E., Wright, A. D., and Clifton, A.: Field-test results using a nacelle-mounted lidar for improving wind turbine power capture by reducing yaw misalignment, in: Journal of Physics: Conference Series, vol. 524, IOP Publishing, 2014.

Fleming, P., Gebraad, P. M., Lee, S., van Wingerden, J.-W., Johnson, K., Churchfield, M., Michalakes, J., Spalart, P., and Moriarty, P.: Simulation comparison of wake mitigation control strategies for a two-turbine case, Wind Energy, 18, 2135–2143, 2015.

Fleming, P., Annoni, J., Shah, J. J., Wang, L., Ananthan, S., Zhang, Z., Hutchings, K., Wang, P., Chen, W., and Chen, L.: Field test of wake steering at an offshore wind farm, Wind Energy Science, 2, 229–239, 2017.

Fleming, P., Annoni, J., Churchfield, M., Martinez-Tossas, L. A., Gruchalla, K., Lawson, M., and Moriarty, P.: A simulation study demonstrating the importance of large-scale trailing vortices in wake steering, Wind Energy Science, 3, 243–255, 2018.

Fleming, P., King, J., Dykes, K., Simley, E., Roadman, J., Scholbrock, A., Murphy, P., Lundquist, J. K., Moriarty, P., Fleming, K., et al.: Initial results from a field campaign of wake steering applied at a commercial wind farm–Part 1, Wind Energy Science, 4, 273–285, 2019.

Fleming, P. A., Ning, A., Gebraad, P. M., and Dykes, K.: Wind plant system engineering through optimization of layout and yaw control, Wind Energy, 19, 329–344, 2016.

Frederik, J. A., Doekemeijer, B. M., Mulders, S. P., and van Wingerden, J.-W.: The helix approach: using dynamic individual pitch control to enhance wake mixing in wind farms, arXiv preprint arXiv:1912.10025, 2019.

Frederik, J. A., Weber, R., Cacciola, S., Campagnolo, F., Croce, A., Bottasso, C., van Wingerden, J.-W., et al.: Periodic dynamic induction control of wind farms: proving the potential in simulations and wind tunnel experiments, Wind Energy Science, 5, 245–257, 2020.

Gebraad, P., Teeuwisse, F., Van Wingerden, J., Fleming, P. A., Ruben, S., Marden, J., and Pao, L.: Wind plant power optimization through yaw control using a parametric model for wake effects—a CFD simulation study, Wind Energy, 19, 95–114, 2016a.

Gebraad, P., Thomas, J. J., Ning, A., Fleming, P., and Dykes, K.: Maximization of the annual energy production of wind power plants by optimization of layout and yaw-based wake control, Wind Energy, 20, 97–107, 2017.

Gebraad, P. M., van Dam, F. C., and van Wingerden, J.-W.: A model-free distributed approach for wind plant control, in: 2013 American Control Conference, pp. 628–633, IEEE, 2013.

Gebraad, P. M., Churchfield, M. J., and Fleming, P. A.: Incorporating atmospheric stability effects into the FLORIS engineering model of wakes in wind farms, in: Journal of Physics: Conference Series, vol. 753, p. 052004, IOP Publishing, 2016b.

Ghaisas, N. S., Ghate, A. S., and Lele, S. K.: Effect of tip spacing, thrust coefficient and turbine spacing in multi-rotor wind turbines and farms, Wind Energy Science, 5, 51–72, 2020.

Ghate, A. S. and Lele, S. K.: Subfilter-scale enrichment of planetary boundary layer large eddy simulation using discrete Fourier–Gabor modes, Journal of Fluid Mechanics, 819, 494–539, 2017.

Goit, J. P. and Meyers, J.: Optimal control of energy extraction in wind-farm boundary layers, Journal of Fluid Mechanics, 768, 5–50, 2015.

Gottlieb, S., Ketcheson, D. I., and Shu, C.-W.: Strong stability preserving Runge-Kutta and multistep time discretizations, World Scientific, 2011.

Grant, I., Parkin, P., and Wang, X.: Optical vortex tracking studies of a horizontal axis wind turbine in yaw using laser-sheet, flow visualisation, Experiments in fluids, 23, 513–519, 1997.

Hansen, K. S., Barthelmie, R. J., Jensen, L. E., and Sommer, A.: The impact of turbulence intensity and atmospheric stability on power deficits due to wind turbine wakes at Horns Rev wind farm, Wind Energy, 15, 183–196, 2012.

Hess, G.: The neutral, barotropic planetary boundary layer, capped by a low-level inversion, 110, 319–355, 2004.

Hoskins, B. J.: The geostrophic momentum approximation and the semi-geostrophic equations, Journal of the Atmospheric Sciences, 32, 233–242, 1975.

Howland, M. F. and Dabiri, J. O.: Wind farm modeling with interpretable physics-informed machine learning, Energies, 12, 2716, 2019.

Howland, M. F. and Yang, X. I.: Dependence of small-scale energetics on large scales in turbulent flows, Journal of Fluid Mechanics, 852, 641–662, 2018.

Howland, M. F., Bossuyt, J., Martínez-Tossas, L. A., Meyers, J., and Meneveau, C.: Wake structure in actuator disk models of wind turbines in yaw under uniform inflow conditions, Journal of Renewable and Sustainable Energy, 8, 043 301, 2016.

Howland, M. F., Ghate, A. S., and Lele, S. K.: Influence of the horizontal component of Earth's rotation on wind turbine wakes, in: Journal of Physics: Conference Series, vol. 1037, IOP Publishing, 2018.

Howland, M. F., Lele, S. K., and Dabiri, J. O.: Wind farm power optimization through wake steering, Proceedings of the National Academy of Sciences, 116, 14 495–14 500, 2019.

Howland, M. F., Ghate, A. S., and Lele, S. K.: Coriolis effects within and trailing a large finite wind farm, in: AIAA Scitech 2020 Forum, p. 0994, 2020a.

Howland, M. F., Ghate, A. S., and Lele, S. K.: Influence of the geostrophic wind direction on the atmospheric boundary layer flow, Journal of Fluid Mechanics, 883, 2020b.

IEA: Energy Technology Perspectives 2017, https://www.iea.org/reports/energy-technology-perspectives-2017, 2017.

Jiménez, Á., Crespo, A., and Migoya, E.: Application of a LES technique to characterize the wake deflection of a wind turbine in yaw, Wind Energy, 13, 559–572, 2010.

Jonkman, J., Butterfield, S., Musial, W., and Scott, G.: Definition of a 5-MW reference wind turbine for offshore system development, Tech. rep., National Renewable Energy Lab.(NREL), Golden, CO (United States), 2009.

Joskow, P. L.: Comparing the costs of intermittent and dispatchable electricity generating technologies, American Economic Review, 101, 238–41, 2011.

Kanev, S.: Dynamic wake steering and its impact on wind farm power production and yaw actuator duty, Renewable Energy, 146, 9–15, 2020.

Kheirabadi, A. C. and Nagamune, R.: A quantitative review of wind farm control with the objective of wind farm power maximization, Journal of Wind Engineering and Industrial Aerodynamics, 192, 45–73, 2019.

Kim, M. and Dalhoff, P.: Yaw Systems for wind turbines–Overview of concepts, current challenges and design methods, in: Journal of Physics: Conference Series, vol. 524, p. 012086, IOP Publishing, 2014.

King, J., Fleming, Paul, K. R., Martínez-Tossas, L. A., Bay, C. J., Mudafort, R., and Simley, E.: Controls-Oriented Model for Secondary Effects of Wake Steering, Wind Energ. Sci. Discuss., in review, pp. https://doi.org/10.5194/wes–2020–3, 2020.

Kingma, D. P. and Ba, J.: Adam: A method for stochastic optimization, arXiv preprint arXiv:1412.6980, 2014.

Knudsen, T., Bak, T., and Svenstrup, M.: Survey of wind farm control—power and fatigue optimization, Wind Energy, 18, 1333–1351, 2015.

Leibovich, S. and Lele, S.: The influence of the horizontal component of Earth's angular velocity on the instability of the Ekman layer, Journal of Fluid Mechanics, 150, 41–87, 1985.

Liew, J. Y., Urbán, A. M., and Andersen, S. J.: Analytical model for the power-yaw sensitivity of wind turbines operating in full wake, Wind Energy Science, 5, 427–437, 2020.

Lin, M. and Porté-Agel, F.: Large-Eddy Simulation of Yawed Wind-Turbine Wakes: Comparisons with Wind Tunnel Measurements and Analytical Wake Models, Energies, 12, 4574, 2019.

Lissaman, P.: Energy effectiveness of arbitrary arrays of wind turbines, Journal of Energy, 3, 323–328, 1979.

Lukassen, L. J., Stevens, R. J., Meneveau, C., and Wilczek, M.: Modeling space-time correlations of velocity fluctuations in wind farms, Wind energy, 21, 474–487, 2018.

Mandel, J.: A brief tutorial on the ensemble Kalman filter, arXiv preprint arXiv:0901.3725, 2009.

Martínez-Tossas, L. A., Churchfield, M. J., and Leonardi, S.: Large eddy simulations of the flow past wind turbines: actuator line and disk modeling, Wind Energy, 18, 1047–1060, 2015.

Martínez-Tossas, L. A., Annoni, J., Fleming, P. A., and Churchfield, M. J.: The aerodynamics of the curled wake: a simplified model in view of flow control, Wind Energy Science (Online), 4, 2019.

Medici, D.: Experimental studies of wind turbine wakes: power optimisation and meandering, Ph.D. thesis, KTH, 2005.

Miao, W., Li, C., Yang, J., and Xie, X.: Numerical investigation of the yawed wake and its effects on the downstream wind turbine, Journal of Renewable and Sustainable Energy, 8, 033 303, 2016.

Mikkelsen, R. et al.: Actuator disc methods applied to wind turbines, Ph.D. thesis, PhD thesis, Technical University of Denmark, 2003.

Mühle, F., Schottler, J., Bartl, J., Futrzynski, R., Evans, S., Bernini, L., Schito, P., Draper, M., Guggeri, A., Kleusberg, E., et al.: Blind test comparison on the wake behind a yawed wind turbine, Wind Energy Science, 3, 883–903, 2018.

Munters, W. and Meyers, J.: An optimal control framework for dynamic induction control of wind farms and their interaction with the atmospheric boundary layer, Philosophical Transactions of the Royal Society A: Mathematical, Physical and Engineering Sciences, 375, 20160 100, 2017.

Munters, W. and Meyers, J.: Dynamic strategies for yaw and induction control of wind farms based on large-eddy simulation and optimization, Energies, 11, 177, 2018.

Munters, W., Meneveau, C., and Meyers, J.: Turbulent inflow precursor method with time-varying direction for large-eddy simulations and applications to wind farms, Boundary-layer meteorology, 159, 305–328, 2016.

Nagarajan, S., Lele, S. K., and Ferziger, J. H.: A robust high-order compact method for large eddy simulation, Journal of Computational Physics, 191, 392–419, 2003.

Niayifar, A. and Porté-Agel, F.: Analytical modeling of wind farms: A new approach for power prediction, Energies, 9, 741, 2016.

Nicoud, F., Toda, H. B., Cabrit, O., Bose, S., and Lee, J.: Using singular values to build a subgrid-scale model for large eddy simulations, 23, 085 106, 2011.

Nordström, J., Nordin, N., and Henningson, D.: The fringe region technique and the Fourier method used in the direct numerical simulation of spatially evolving viscous flows, SIAM Journal on Scientific Computing, 20, 1365–1393, 1999.

Önder, A. and Meyers, J.: On the interaction of very-large-scale motions in a neutral atmospheric boundary layer with a row of wind turbines, Journal of Fluid Mechanics, 841, 1040–1072, 2018.

Ouyang, X. and Lin, B.: Levelized cost of electricity (LCOE) of renewable energies and required subsidies in China, Energy policy, 70, 64–73, 2014.

Park, J. and Law, K. H.: A data-driven, cooperative wind farm control to maximize the total power production, Applied Energy, 165, 151–165, 2016.

Raach, S., Doekemeijer, B., Boersma, S., van Wingerden, J.-W., and Cheng, P. W.: Feedforward-Feedback wake redirection for wind farm control, Wind Energ. Sci. Discuss., https://doi.org/10.5194/wes-2019-54, in review, 2019.

Schreiber, J., Bottasso, C. L., Salbert, B., , and Campagnolo, F.: Improving wind farm flow models by learning from operational data, Wind Energ. Sci. Discuss., https://doi.org/10.5194/wes-2019-91, in review, 2019.

Senoner, J.-M., García, M., Mendez, S., Staffelbach, G., Vermorel, O., and Poinsot, T.: Growth of rounding errors and repetitivity of large eddy simulations, AIAA journal, 46, 1773–1781, 2008.

Shapiro, C. R., Meyers, J., Meneveau, C., and Gayme, D. F.: Dynamic wake modeling and state estimation for improved model-based receding horizon control of wind farms, in: 2017 American Control Conference (ACC), pp. 709–716, IEEE, 2017.

Shapiro, C. R., Gayme, D. F., and Meneveau, C.: Modelling yawed wind turbine wakes: a lifting line approach, Journal of Fluid Mechanics, 841, 2018.

Shapiro, C. R., Starke, G. M., Meneveau, C., and Gayme, D. F.: A Wake Modeling Paradigm for Wind Farm Design and Control, Energies, 12, 2956, 2019.

Stevens, R. J. and Meneveau, C.: Flow structure and turbulence in wind farms, Annual review of fluid mechanics, 49, 2017.

Taylor, G. I.: The spectrum of turbulence, Proceedings of the Royal Society of London. Series A-Mathematical and Physical Sciences, 164, 476–490, 1938.

Vali, M., Petrović, V., Boersma, S., van Wingerden, J.-W., Pao, L. Y., and Kühn, M.: Adjoint-based model predictive control for optimal energy extraction in waked wind farms, Control Engineering Practice, 84, 48–62, 2019.

Wiser, R., Lantz, E., Mai, T., Zayas, J., DeMeo, E., Eugeni, E., Lin-Powers, J., and Tusing, R.: Wind vision: A new era for wind power in the United States, The Electricity Journal, 28, 120–132, 2015.

Wyngaard, J. C.: Turbulence in the Atmosphere, Cambridge University Press, 2010.

Yang, X. I. and Howland, M. F.: Implication of Taylor's hypothesis on measuring flow modulation, Journal of Fluid Mechanics, 836, 222–237, 2018.